

Smoothing Variances Across Time: Adaptive Stochastic Volatility

Jason B. Cho*

Department of Statistics and Data Science, Cornell University
and

David S. Matteson

Department of Statistics and Data Science, Cornell University

June 13, 2025

Abstract

We introduce a novel Bayesian framework for estimating time-varying volatility by extending the Random Walk Stochastic Volatility (RWSV) model with Dynamic Shrinkage Processes (DSP) in log-variances. Unlike the classical Stochastic Volatility (SV) or GARCH-type models with restrictive parametric stationarity assumptions, our proposed Adaptive Stochastic Volatility (ASV) model provides smooth yet dynamically adaptive estimates of evolving volatility and its uncertainty. We further enhance the model by incorporating a nugget effect, allowing it to flexibly capture small-scale variability while preserving smoothness elsewhere. We derive the theoretical properties of the global-local shrinkage prior DSP. Through simulation studies, we show that ASV exhibits remarkable misspecification resilience and low prediction error across various data-generating processes. Furthermore, ASV's capacity to yield locally smooth and interpretable estimates facilitates a clearer understanding of the underlying patterns and trends in volatility. As an extension, we develop the Bayesian Trend Filter with ASV (BTF-ASV) which allows joint modeling of the mean and volatility with abrupt changes. Finally, our proposed models are applied to time series data from finance, econometrics, and environmental science, highlighting their flexibility and broad applicability.

Keywords: Stochastic Volatility; Bayesian Smoothing; Bayesian State-Space Model; Global-Local Shrinkage Prior

*The authors gratefully acknowledge financial support from *National Science Foundation grants OAC-1940124 and DMS-2114143*

1 Introduction

Volatility of a time series quantifies deviations from the mean and is fundamental to understanding the underlying data-generating process. In finance, volatility estimation is essential for pricing, risk assessment, and asset management [Bollerslev, 1986, Hull and White, 1987]. In epidemiology, it aids in early outbreak detection and forecasting new cases of diseases [Achcar et al., 2020, Kostoulas et al., 2021, Sarkar and Chatterjee, 2017]. Climate science measures volatility to study phenomena like tornadoes, droughts, and rainfall [Mehdizadeh et al., 2017, Modarres and Ouarda, 2014, Tippett, 2014]. In engineering, volatility helps predict mechanical failures [Ma et al., 2017, Pham and Yang, 2010], while in hydrology, it informs understanding of streamflow variations [Otache, 2012, Wang et al., 2023a,b, 2005].

Classical volatility models include Autoregressive Conditional Heteroskedasticity (ARCH) [Engle, 1982], Generalized ARCH (GARCH) [Bollerslev, 1986], and Stochastic Volatility (SV) [Hull and White, 1987, Melino and Turnbull, 1990, Taylor, 2008]. They all make the stationarity assumption that the unconditional variance is constant. However, a growing body of econometric literature points to evolving volatility patterns in stock markets around the world [Chou, 1988, French et al., 1987, Nishino and Kakamu, 2015, Poon and Taylor, 1992, So et al., 1997, Su and Wang, 2020]. Moreover, the stationarity assumption is often unrealistic in fields like climate science and epidemiology, due to climate change and seasonal or outbreak-driven dynamics [Kostoulas et al., 2021, Tippett, 2014].

Figure 1 illustrates evolving volatility patterns in three real-world datasets: weekly log-returns of the S&P 500 index, daily electricity demand in New York State, and daily bike rental counts via Capital Bikeshare. All three exhibit nonstationary volatility patterns. In

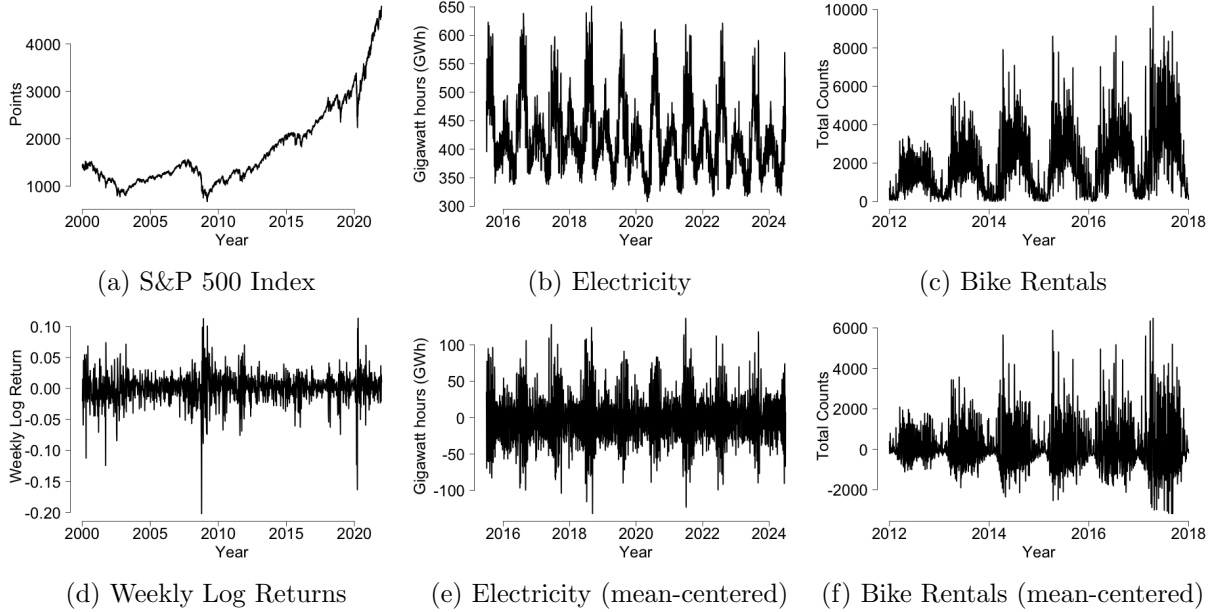


Figure 1: Figures 1a to 1c display the S&P 500 index from 2012-01-01 to 2021-12-31, daily total electricity demand (in gigawatt hours) in New York State from 2015-07-01 to 2024-06-30, and daily bike rental counts via Capital Bikeshare by non-members in Washington metropolitan area from 2012-01-01 to 2017-12-31, respectively. Figures 1d to 1f show the corresponding mean-centered series: weekly log returns for the S&P 500 index with the average log return subtracted, and series for electricity demand and bike rentals mean-centered using smoothing spline, respectively. The S&P 500 index data are obtained using the `quantmod` package in R [Ryan and Ulrich, 2024] from Yahoo Finance [Finance, 2025], electricity demand data from the New York Independent System Operator (NYISO) [EIA, 2024], and bike rental data from Capital Bikeshare [Bikeshare, 2024].

Figures 1a and 1d, persistent periods of high and low volatility reflect changing market conditions. In Figures 1b, 1c, 1e and 1f, both electricity and bike data show seasonal cycles in both mean and volatility, with elevated volatility during high-demand periods.

Existing approaches address such patterns by incorporating hidden Markov switching (HMS) structure into existing SV and GARCH models [Ardia et al., 2018, Bauwens et al., 2010, Brunetti et al., 2008, Cai, 1994, Gray, 1996a, Hamilton and Susmel, 1994, Hwang et al., 2004, So et al., 1998]. However, HMS models suffer from three major limitations: they (1) require specification of the number of regimes, which is typically unknown; (2) are computationally intensive as pointed out in Gray [1996b] and Billio et al. [2016]; and (3) impose a discrete regime-switching structure, which may not capture ever evolving

volatility dynamics. For example, Figure 1f reveals a seasonal increase in volatility for bike rentals, with the magnitude of these fluctuations growing over time. For example, volatility in 2012 is substantially lower than in 2017. Such a pattern is difficult to reconcile with a model based on a fixed number of regimes, as it reflects a continuous evolution of volatility rather than discrete shifts.

We introduce the Adaptive Stochastic Volatility (ASV) model as an extension of the Random Walk Stochastic Volatility (RWSV) model [Harvey et al., 1994, Ruiz, 1994]. RWSV assumes the log-variance of the observed process follows a Gaussian random walk with a constant variance. In contrast, ASV introduces two significant modifications to RWSV: it incorporates a time-varying variance for the log-variance increments and adopts a global-local shrinkage prior for adaptability. For the shrinkage prior, we specifically highlight a class of prior distributions called Dynamic Shrinkage Processes (DSP) by Kowal et al. [2019], as it provides a flexible framework for adaptive shrinkage for time series. To further improve robustness, we also consider a nugget variant of ASV, which adds an additional Gaussian noise to capture local fluctuations not explained by the smooth latent process.

The standout feature of our proposed model is its local adaptability, effectively estimating volatility in the presence of both gradual and abrupt changes in the volatility process with notable smoothness in between. It allows robustness against model misspecification, resulting in low prediction error across diverse data-generating processes (DGPs). In addition, ASV’s smooth volatility estimates provide clearer insights into the underlying patterns and trends. The model also naturally highlights periods of heightened volatility variation, offering additional interpretability in identifying structural shifts.

The remainder of this paper is organized as follows. Section 2 first introduces DSP and its theoretical properties, followed by a description of our proposed model (ASV)

and its associated parameters. Section 3 provides an overview of the data augmentation techniques for efficient Gibbs sampling scheme; full conditional distributions are detailed in the supplementary material. Simulation study results are summarized in Section 4. Section 5 presents empirical analyses on three real-world datasets: the S&P 500 index, daily electricity usage in New York, and bike rental counts. In Section 6, the Bayesian Trend Filter with ASV (BTF-ASV), which jointly estimates the time-varying means and the variances, is proposed as an extension and applied to the sunspot number data.

2 Methodology

2.1 The Random Walk Stochastic Volatility Model

ASV may be viewed as an extension of RWSV [Harvey et al., 1994, Ruiz, 1994]. Consider a zero mean process with T observations, $\{y_t\}_{t=1}^T$, and its log-variance term $\{h_t\}_{t=1}^T$. SV assumes the observed process y_t to follow a normal distribution with its log-variance term, h_t , following the lag order 1 autoregression. RWSV is a special case of SV in which the autoregressive coefficient is fixed at 1. Thus, the model is defined as:

$$\begin{aligned} y_t &= \exp\{h_t/2\}\epsilon_t & [\epsilon_t] &\stackrel{iid}{\sim} N(0, 1), \\ [\Delta h_t | \sigma_h^2] &\sim N(0, \sigma_h^2) & [\sigma_h^2] &\sim \pi(\sigma_h^2). \end{aligned} \tag{1}$$

In RWSV, h_t is governed by a time-invariant variance term σ_h^2 , which determines the degree of variation between successive log-variances. A large σ_h^2 implies high probability of significant changes in the h_t process, whereas a small σ_h^2 indicates high probability of minimal to no changes in h_t . In a frequentist framework, σ_h is treated as a fixed parameter, often estimated via quasi-maximum likelihood [Harvey et al., 1994, Ruiz, 1994]. A more

recent study by Nishino and Kakamu [2015] employs a Bayesian framework for estimation with a non-informative inverse-gamma priors for $\pi(\sigma_h^2)$.

2.2 Stochastic Volatility with Local Only Shrinkage

RWSV may fit poorly when the time series exhibits both significant and minimal changes, as it assumes a time-invariant innovation variance σ_h^2 . Ideally, we would prefer σ_h^2 to adapt over time, remaining small during stable periods and increasing during periods of abrupt changes in h_t . A natural approach to address this limitation is to introduce sparsity in the variance process. Under the frequentist framework, sparsity in Δh_t may be attained by imposing a penalty, such as the ℓ_1 penalty used in LASSO [Tibshirani, 1996]. In a Bayesian setting, near sparsity can be imposed via heavy-tailed priors on the variance parameter. Motivated by the Bayesian LASSO [Park and Casella, 2008] and the scale-mixture Gaussian representation of the Laplace distribution [West, 1987], we propose an intermediate model, RWSV with Bayesian LASSO (RWSV-BL):

$$\begin{aligned} y_t &= \exp\{h_t\}\epsilon_t & [\epsilon_t] &\stackrel{iid}{\sim} N(0, 1), \\ [\Delta h_t | \sigma_{h,t}^2] &\sim N(0, \sigma_{h,t}^2 | \Lambda) & [\sigma_{h,t}^2] &\stackrel{iid}{\sim} \text{Exp}\{(2\Lambda^2)^{-1}\}, \end{aligned} \tag{2}$$

where $\Lambda > 0$ is a hyperparameter controlling the prior concentration. Following Park and Casella [2008], we place a Gamma prior on Λ^2 for full Bayesian inference. Under RWSV, $\sigma_{h,t}^2$ induces shrinkage by encouraging most increments to be small, while still allowing occasional large deviations.

2.3 Dynamic Shrinkage Processes and their Properties

Before introducing the proposed model, we first describe a class of global-local shrinkage priors known as DSP, a central component in our formulation. Global-local shrinkage priors have been widely studied for Gaussian observations, particularly in high-dimensional regression. Notable examples include the horseshoe prior [Carvalho et al., 2010], the horseshoe+ prior [Bhadra et al., 2015], and the triple gamma prior [Cadonna et al., 2019]. Among these, DSP offers a particularly flexible formulation that generalizes several existing priors and naturally incorporates temporal dependence.

DSP has shown versatility across various applications. For example, Wu et al. [2024a] integrate DSP into a Bayesian dynamic linear model to estimate change points and score outliers. Schafer and Matteson [2024] apply it to construct the negative binomial Bayesian trend filter (NB-BTF) for adaptively smoothing integer-valued time series. Additionally, Wu et al. [2024b] combine the Bayesian trend filter with DSP and a machine learning-based regularization method to effectively distinguish micro-level drifts from macro-level shifts.

DSP serves as a prior for time-varying log-variance parameters. Define $v_t := \log(\sigma_{h,t}^2)$, where $v_t | \mu, \phi \sim DSP(a, b, \mu, \phi)$. DSP imposes an autoregressive structure on $\{v_t\}_{t=1}^T$, allowing for locally adaptive shrinkage through heavy-tailed innovations around a persistent mean process:

$$v_t := \log(\sigma_{h,t}^2) = \mu + \phi(v_{t-1} - \mu) + \eta_t \quad [\eta_t] \stackrel{iid}{\sim} Z(a, b, 0, 1), \quad (3)$$

where Z -distribution has the following density function [Barndorff-Nielsen et al., 1982]:

$$f(z|a, b, \mu_z, \sigma_z) = (\sigma_z B(a, b))^{-1} \left(\exp \left\{ \frac{z - \mu_z}{\sigma_z} \right\} \right)^a \left(1 + \exp \left\{ \frac{z - \mu_z}{\sigma_z} \right\} \right)^{-(a+b)}.$$

For fully Bayesian inference, we place weakly informative priors on μ and ϕ , and describe them in detail in Section 3. Under this framework, the global parameter is defined as $\tau = \exp\{\mu(1 - \phi)/2\}$ and the local shrinkage parameter is defined as $\lambda_t = \exp\{(\phi v_{t-1} + \eta_t)/2\}$. The autoregressive coefficient $|\phi| < 1$ controls temporal dependence in local shrinkage. When ϕ is close to 1, the process exhibits strong positive dependence: strong shrinkage tends to be followed by continued strong shrinkage, and weak shrinkage by weak shrinkage. When ϕ is close to -1, the process favors alternation between strong and weak shrinkage across time.

The Z -distribution on the local scale parameter η_t governs the degree of local shrinkage at each time t . In our simulation study (Section 4) and empirical study (Section 5), we consider two specific instances of DSP. When $a = b = 1/2$ and the autoregressive coefficient $\phi = 0$, the prior reduces to the well-known horseshoe prior (HS) [Carvalho et al., 2010], since $\lambda_t = \exp\{\eta_t/2\} \sim C^+(0, 1)$. When ϕ is estimated from the data with $a = b = 1/2$, the prior induces temporal dependence in shrinkage and is referred to as the dynamic horseshoe (DHS) prior [Kowal et al., 2019]. Other special cases of DSP include the Strawderman–Berger prior when $a = 1/2$ and $b = 1$ [Strawderman, 1971], the normal–exponential–gamma prior when $a = 1$ and $b > 2$ [Griffin and Brown, 2005], and the Jeffreys prior with $a = b \rightarrow 0$ [Figueiredo, 2003].

While DSP has an appealing formulation and a clear connection to well-known priors, its theoretical properties remain incomplete. In particular, DSP distinguishes itself from other global-local shrinkage priors by introducing temporal dependence in the local shrinkage parameter λ_t . Due to the time dependence, the original work by Kowal et al. [2019] focuses on the conditional behavior while the properties of the marginal distribution remain unexamined. We derive new results on the stationary distribution of DSP.

Define $z_{t,h} := \phi^h \eta_{t-h}$. Infinite-order moving average representation of v_t results in $v_t = \mu + \phi(v_{t-1} - \mu) + \eta_t = \mu + \sum_{h=0}^{\infty} z_{t,h}$, with $\eta_t \stackrel{iid}{\sim} Z(1/2, 1/2, 0, 1)$. As shown in Barndorff-Nielsen et al. [1982], $z_{t,h}$ is a scaled hyperbolic secant distribution, with $\mathbb{E}(z_{t,h}|\phi) = 0$ and $\text{Var}(z_{t,h}|\phi) = (|\phi|^h \pi)^2$. Consider $z_t := \sum_{h=0}^{\infty} z_{t,h}$.

Theorem 1. *z_t converges almost surely if and only if $|\phi| < 1$.*

Proof. This directly follows from Kolmogorov's three series theorem. Note that the variance $\sum_{h=0}^{\infty} \text{Var}(z_{t,h}|\phi)$ converges if and only if $|\phi| < 1$. Exact derivation is explored in Appendix A.1. \square

Corollary 1.1. *When $|\phi| < 1$,*

$$\begin{aligned}\mathbb{E}(z_t|\phi) &= \mathbb{E}\left(\sum_{h=0}^{\infty} z_{t,h}|\phi\right) = \sum_{h=0}^{\infty} \mathbb{E}(z_{t,h}|\phi) = 0. \\ \text{Var}(z_t|\phi) &= \text{Var}\left(\sum_{h=0}^{\infty} z_{t,h}|\phi\right) = \sum_{h=0}^{\infty} \text{Var}(z_{t,h}|\phi) = \sum_{h=0}^{\infty} \pi^2 \phi^{2h} = \frac{\pi^2}{1 - \phi^2}.\end{aligned}$$

Characteristic function of $z_{h,t}$ is $\text{sech}(\pi\phi^h t)$. Thus, the characteristic function, $g(t)$, for $\sum_{h=0}^{\infty} z_{h,t}$, would be an infinite product of the characteristic function of $z_{h,t}$.

$$g(t) = \prod_{h=0}^{\infty} \text{sech}(\pi\phi^h t), \quad -\frac{1}{2} < t < \frac{1}{2}.$$

Similarly, for the moment generating function $M(t)$

$$M(t) = \prod_{h=0}^{\infty} \sec(\pi\phi^h t), \quad -\frac{1}{2} < t < \frac{1}{2}.$$

Theorem 2. *If $|\phi| = 0.5$, $\eta_{t-h} \stackrel{iid}{\sim} Z(1/2, 1/2, 0, 1)$, and $z_{t,h} := \phi^h \eta_{t-h}$, then $z_t := \sum_{h=0}^{\infty} z_{t,h} \xrightarrow{a.s} \text{Logistic}(0, 2)$.*

Proof. Derivations are explored in Appendix A.2. \square

Thus, assuming $\mu = 0$ and $\phi = 0.5$ for simplicity, we have the following density function for v_t , $\lambda_t := \exp\{v_t/2\}$ and $\kappa_t := \frac{1}{1+\exp\{v_t\}}$ for the stationary distribution of DSP:

$$f(v_t) = \frac{1}{8} \operatorname{sech}^2\left(\frac{v_t}{4}\right),$$

$$f(\lambda_t) = \frac{1}{4\lambda_t} \operatorname{sech}^2\left(\frac{\log(\lambda_t)}{2}\right) = \frac{1}{(1+\lambda_t)^2},$$

$$f(\kappa_t) = \frac{1}{8(\kappa_t)(1-\kappa_t)} \operatorname{sech}^2\left(\frac{1}{4}\left(\log\left(\frac{1-\kappa_t}{\kappa_t}\right)\right)\right) = \frac{1}{\sqrt{\kappa_t(1-\kappa_t)}} \frac{1}{2\kappa_t(1+\sqrt{\frac{1-\kappa_t}{\kappa_t}})^2}.$$

Figure 2 compares the prior distribution of λ_t and κ_t for the horseshoe and DSP. The

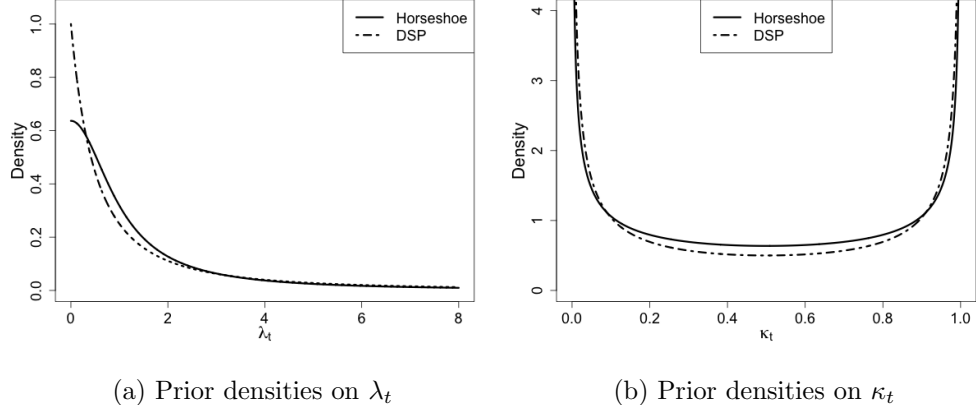


Figure 2: Prior densities of λ_t and κ_t under the horseshoe prior and the stationary distribution of Dynamic Shrinkage Process (DSP) with $\eta_t \stackrel{iid}{\sim} Z(1/2, 1/2, 0, 1)$, $\phi = 1/2$ and $\mu = 0$.

horseshoe prior in Carvalho et al. [2010] assumes $\lambda_t \sim C^+(0, 1)$ and $\kappa_t \sim Beta(1/2, 1/2)$.

The density function of $g(\lambda_t)$ and $g(\kappa_t)$ under the horseshoe are:

$$g(\lambda_t) = \frac{2}{\pi(1+\lambda_t^2)}, \quad g(\kappa_t) = \frac{1}{\pi\sqrt{\kappa_t(1-\kappa_t)}}.$$

For λ_t , the density function for DSP has heavier tails and a sharper spike at zero. Specifically, $f(\lambda_t) > g(\lambda_t)$ when $\lambda_t \in (0, \frac{2-\sqrt{(4-\pi)\pi}}{(\pi-2)}) \cup (\frac{2+\sqrt{(4-\pi)\pi}}{(\pi-2)}, \infty)$. In terms of κ_t , the DSP

prior puts more weight around 0 and 1 than the horseshoe. This is due to the extra U-shaped term in κ_t , $1/(2\kappa_t(1 + \sqrt{\frac{1-\kappa_t}{\kappa_t}})^2)$, pushing the mass of the distribution to near 0 and 1.

Finally, the marginal prior on Δh is considered:

Theorem 3. Let $|\phi| = 0.5$, $\eta_{t-h} \stackrel{iid}{\sim} Z(1/2, 1/2, 0, 1)$, $z_{t,h} := \phi^h \eta_{t-h}$, $v_t := \sum_{h=0}^{\infty} z_{t,h}$, $\lambda_t := \exp\{v_t/2\}$ and $\Delta h_t \sim N(0, \lambda_t)$,

$$\lim_{\Delta h_t \rightarrow 0} f(\Delta h_t) = \infty,$$

$$K_L \log(1 + \frac{4}{\Delta^2 h_t}) < f(\Delta h_t) < K_U \log(1 + \frac{2}{\Delta^2 h_t}), \quad |\Delta h_t| > 0$$

where $K_U = \frac{1}{2\sqrt{2\pi}}$ and $K_L = \frac{1}{8\sqrt{2\pi}}$

Proof. The proof is similar to Theorem 1 in Carvalho et al. [2010]. We use the fact that $\forall x > 0$,

$$\frac{1}{2(1+x^2)} \leq \frac{1}{(1+x)^2} \leq \frac{1}{(1+x^2)}.$$

Derivation is detailed in Appendix A.3. □

The bounds for the marginal distribution of DSP are similar to the ones from the horseshoe with the only difference being the constant factor K_L and K_U . Under the horseshoe prior, $K_U = \frac{1}{\sqrt{2\pi^3}}$ and $K_L = \frac{1}{2\sqrt{2\pi^3}}$. Like horseshoe prior, DSP is also unbounded near the origin, which leads to super-efficiency in a sparse setting as shown in Carvalho et al. [2010].

2.4 Adaptive Stochastic Volatility via Global-Local Shrinkage

We propose ASV, which uses DSP explored in Section 2.3, to adaptively estimate time-varying volatility in a smooth yet locally adaptive manner. In ASV, the prior models the

log-variance of the k th-order differences of h_t : $\Delta^k h_t | \sigma_{h,t}^2 \sim N(0, \sigma_{h,t}^2)$. As previously defined, $v_t := \log(\sigma_{h,t}^2)$ follows an autoregressive structure described in Equation 3. Unlike RWSV-BL, ASV incorporates both the global parameter $\mu(1-\phi)$ and the local parameter $\phi v_{t-1} + \eta_t$. The global parameter promotes overall smoothness, while the local parameter preserves local adaptivity. The resulting model, ASV, has the following hierarchical representation:

$$\begin{aligned} y_t &= \exp\{h_t\} \epsilon_t & [\epsilon_t] &\stackrel{iid}{\sim} N(0, 1), \\ [\Delta^k h_t | \sigma_{h,t}^2] &\sim N(0, \sigma_{h,t}^2) & [\log(\sigma_{h,t}^2) | \mu, \phi] &\sim DSP(a, b, \mu, \phi). \end{aligned} \tag{4}$$

The differencing order k plays a central role in controlling the model's smoothness. ASV can be viewed as a variance-process analogue of smoothing methods for the mean function, such as the Bayesian Trend Filter by Roualdes [2015] and Kowal et al. [2019], Hodrick-Prescott filter by Hodrick and Prescott [1997], ℓ_1 -trend filter by Kim et al. [2009] and Tibshirani [2014], and a smoothing spline. Penalizing the k th-order difference encourages the underlying signal to be locally well-approximated by a polynomial of degree $k - 1$: $k = 1$ promotes piecewise constant behavior, $k = 2$ encourages piecewise linearity, and higher-order penalties induce smoother trends. In our study, we use $k = 1$, consistent with traditional volatility models like GARCH and SV, which typically assume stationary dynamics with abrupt clustering. Nevertheless, higher-order differencing may be better suited for applications with more gradually evolving volatility.

In practice, volatility processes may exhibit both local irregularities that are neither smooth nor abrupt. To account for this, we extend ASV by introducing a nugget effect, an additional noise term that absorbs small scale local fluctuations. We refer to this model as

ASV with nugget:

$$\begin{aligned}
h_t &= h_t^* + u_t & [u_t | \sigma_c^2] &\sim N(0, \sigma_c^2), \\
& & [\Delta^k h_t^* | \sigma_{h,t}^2] &\sim N(0, \sigma_{h,t}^2) & [\log(\sigma_{h,t}^2) | \mu, \phi] &\sim DSP(a, b, \mu, \phi).
\end{aligned} \tag{5}$$

ASV with nugget described in Equation 5 shares the same observation model in Equation 4, but differs in that the log-variance h_t is now decomposed into a smooth component h_t^* and a local noise term u_t , allowing the model to capture both structured and unstructured variation.

3 Bayesian Inference via Data Augmentation

We briefly discuss the Bayesian inference procedure for the ASV model described in Equation 4. The observed data are denoted by $\mathbf{y} := (y_1, \dots, y_T)'$, the latent log-variance process by $\mathbf{h} := (h_1, \dots, h_T)'$ and its associated log-variance process by $\mathbf{v} := (\log(\sigma_{h,1}^2), \dots, \log(\sigma_{h,T}^2))'$. For the autoregressive parameter ϕ , a shifted Beta prior: $(\phi + 1)/2 \sim Beta(1/2, 1/2)$ is assumed. For the global location parameter, we assume $\mu \sim Z(1/2, 1/2, 0, 1)$, which implies $\tau = \exp\{\mu(1 - \phi)/2\} \sim C^+(0, 1)$ when $\phi = 0$. This recovers the global scale prior used in the horseshoe formulation by Carvalho et al. [2010]. Inference proceeds by sampling from the joint posterior distribution of $(\mathbf{h}, \mathbf{v}, \mu, \phi)$ conditional on \mathbf{y} via Gibbs sampling scheme that iteratively samples from the full conditional distributions.

Sampling from the conditional posterior distribution of \mathbf{h} in the SV model is challenging due to its non-linear likelihood. While methods like sequential Monte Carlo by Jacquier et al. [1994] can sample h_t from the exact conditional posterior sequentially, this approach is computationally demanding. Instead, we adopt a quasi-likelihood approach based on the transformed observations $\mathbf{y}^* := (\log(y_1^2), \dots, \log(y_T^2))'$, recasting the model into a linear

system with a non-Gaussian error term: $y_t^* = h_t + \log(\epsilon_t^2)$, $\epsilon_t \stackrel{iid}{\sim} N(0, 1)$.

The asymmetric error term $\log(\epsilon_t^2)$ can be accurately approximated by a finite Gaussian mixture. The idea is originally proposed by Kim et al. [1998] and later refined by Omori et al. [2007], who introduced a 10-component Gaussian mixture approximation:

$$\log(\epsilon_t^2) \approx m_{j_t} + o_t \quad [o_t] \stackrel{iid}{\sim} N(0, w_{j_t}^2),$$

where $j_t \stackrel{iid}{\sim} \text{Categorical}(\pi^{\text{Omori}})$, with fixed weights $\pi^{\text{Omori}} = (\pi_1, \dots, \pi_{10})$. Each latent index $j_t \in \{1, \dots, 10\}$ selects a component-specific mean m_{j_t} and standard deviation w_{j_t} from a pre-specified table [Omori et al., 2007]. This approximation transforms the quasi-likelihood into a conditionally Gaussian model, making posterior sampling significantly more efficient. Conditional on j_t , the full conditional distribution of \mathbf{h} becomes a Gaussian likelihood with a structured Gaussian prior:

$$y_t^* \approx h_t + m_{j_t} + o_t \quad [o_t | s_{j_t}] \stackrel{ind}{\sim} N(0, w_{j_t}^2),$$

$$[\Delta^k h_t | v_t] \sim N(0, \exp(v_t)) \quad [v_t | \mu, \phi] \sim DSP(a, b, \mu, \phi).$$

The same Gaussian mixture approximation and data augmentation are applied to $\log((\Delta^k h_t)^2)$, which shares the same distribution as y^* . A corresponding latent variable s_t is introduced.

The evolution equation of v_t in Equation 3 may be interpreted as the SV model with a heavy-tailed noise distribution $\eta_t \sim Z(a, b, 0, 1)$. We leverage the Pólya-Gamma scale mixture representation of the Z -distribution [Barndorff-Nielsen et al., 1982], which states:

$$[\eta_t | \xi_t] \sim N(\xi_t^{-1}(a - b)/2, \xi_t^{-1}) \quad [\xi_t] \sim PG(a + b, 0).$$

Combined with the approximation on $\log(\Delta^k h_t^2)$, the log-variance evolution becomes con-

ditionally Gaussian:

$$\log((\Delta^k h_t)^2) \approx v_t + m_{st} + r_t \quad [r_t | w_{st}] \stackrel{ind}{\sim} N(0, w_{st}^2),$$

$$v_t = \mu + \phi(v_{t-1} - \mu) + \eta_t \quad [\eta_t | \xi_t] \stackrel{ind}{\sim} N(\xi_t^{-1}(a - b)/2, \xi_t^{-1}).$$

We sample \mathbf{v} using the efficient AWOL sampler proposed by Kastner and Frühwirth-Schnatter [2014]. Sampling from the Pólya-Gamma distribution is performed by truncating an infinite sum as shown in [Polson et al., 2013]. Similarly, $\xi_\mu \sim PG(1, 0)$ is introduced to represent $\mu \sim Z(1/2, 1/2, 0, 1)$ as $\mu | \xi_\mu \sim N(0, \xi_\mu^{-1})$.

In addition to the four existing parameters $(\mathbf{h}, \mathbf{v}, \mu, \phi)$, four additional parameters are introduced: the mixture indicators $\mathbf{j} := (j_1, \dots, j_T)'$ and $\mathbf{s} := (s_1, \dots, s_T)'$, and the Pólya-Gamma variables: $\boldsymbol{\xi} := (\xi_1 \dots \xi_T)'$ and ξ_μ . This section shows how the data augmentation framework enables efficient posterior sampling of \mathbf{h} and \mathbf{v} . Detailed derivations of the full conditional distributions are discussed in the Appendix B.

For the nugget model described in Equation 5, the same approximation and data augmentation are applied. An additional Gaussian layer $h_t | h_t^*, \sigma_c^2 \sim N(h_t^*, \sigma_c^2)$ is introduced and the prior is placed on $\Delta^k h_t^*$ instead of $\Delta^k h_t$. However, the resulting model remains conditionally Gaussian, and the structure of the Gibbs sampler remains largely unchanged.

4 Simulation Study

4.1 Set-up

The simulation study evaluates the performance of the proposed ASV model against several existing methods, including the SV, Markov-Switching SV with two regimes (MSSV2), RWSV, GARCH, and two-regime GARCH (MSGARCH2). A local-only shrinkage model

DGP1: SV with 1 Regime	DGP2: SV with 2 Regimes
$y_t \sim N(0, \exp(h_t))$ $h_t = 3 + 0.8(h_{t-1} - 3) + 0.2u_t$ $u_t \stackrel{iid}{\sim} N(0, 1)$	$y_t \sim N(0, \exp(h_t))$ $h_t = m_{s_t} + 0.8(h_{t-1} - m_{s_{t-1}}) + 0.2u_t$ $u_t \stackrel{iid}{\sim} N(0, 1)$ $m_{s_t} = \begin{cases} -10, & \text{if } s_t = 0. \\ 6, & \text{if } s_t = 1. \end{cases}$
DGP3: SV with 3 Regimes	DGP4: GARCH with 1 Regime
$y_t \sim N(0, \exp(h_t))$ $h_t = m_{s_t} + 0.8(h_{t-1} - m_{s_{t-1}}) + 0.2u_t$ $u_t \stackrel{iid}{\sim} N(0, 1)$ $m_{s_t} = \begin{cases} -10, & \text{if } s_t = 0. \\ -3, & \text{if } s_t = 1. \\ 3, & \text{if } s_t = 2. \end{cases}$	$y_t \sim N(0, \sigma_{y,t}^2)$ $\sigma_{y,t}^2 = 1 + 0.1y_{t-1}^2 + 0.5\sigma_{y,t-1}^2$
DGP5: GARCH with 2 Regimes	DGP6: GARCH with 3 Regimes
$y_t \sim N(0, \sigma_{y,t}^2)$ $\sigma_{y,t}^2 = m_{s_t} + 0.15y_{t-1}^2 + \beta_{s_t}\sigma_{y,t-1}^2$ $m_{s_t} = \begin{cases} 8, & \text{if } s_t = 0. \\ 0.1, & \text{if } s_t = 1. \end{cases}$ $\beta_{s_t} = \begin{cases} 0.8, & \text{if } s_t = 0. \\ 0.3, & \text{if } s_t = 1. \end{cases}$	$y_t \sim N(0, \sigma_{y,t}^2)$ $\sigma_{y,t}^2 = m_{s_t} + 0.15y_{t-1}^2 + \beta_{s_t}\sigma_{y,t-1}^2$ $m_{s_t} = \begin{cases} 12, & \text{if } s_t = 0. \\ 8, & \text{if } s_t = 1. \\ 0.1, & \text{if } s_t = 2. \end{cases}$ $\beta_{s_t} = \begin{cases} 0.8, & \text{if } s_t = 0. \\ 0.5, & \text{if } s_t = 1. \\ 0.2, & \text{if } s_t = 2. \end{cases}$
DGP7: Sinusoidal	DGP8: Piecewise Constant
$y_t \sim \mathcal{N}(0, \exp(h_t))$ $h = A \sin(10(2\pi t)/T) + B \cos(10(2\pi t)/T) + C \sin(3(2\pi t)/T) + D \cos(3(2\pi t)/T)$ $A, B, C, D \stackrel{iid}{\sim} U(0, 5)$	$y_t \sim \mathcal{N}(0, \exp(h_t))$ $j := \left\lfloor \frac{t}{25} \right\rfloor + 1$ $h_t = (-1)^j \cdot z_j $ $z_j \sim \begin{cases} N(5, 0.5^2) & \text{if } j \text{ is even} \\ N(0, 0.5^2) & \text{if } j \text{ is odd} \end{cases}$

Table 1: Summary of the eight data-generating processes (DGP). DGP 1 - 3 simulate a stochastic-volatility model with 1, 2, or 3 regimes; DGP 4-6 simulate a GARCH(1,1) model with 1, 2, or 3 regimes. In DGP 7, h_t is a random sinusoid; in DGP 8, h_t is piecewise constant with random intercepts. For DGPs 2 and 4, the transition probability of remaining in the same state is 0.98, and transitioning to a different state is 0.02. For DGPs 3 and 6, the probability of staying in the same state is 0.98, while switching to any other state occurs with probability 0.01. Each DGP comprises 1,000 sample paths, each path being 1,000 data points in length.

RWSV-BL is also included for comparison. Four variants of ASV: ASV with the horseshoe prior (ASV-HS), ASV with the dynamic horseshoe prior (ASV-DHS), and their respective versions with a nugget effect (ASV-HS-N and ASV-DHS-N) are considered. ASV-HS corresponds to the special case of Equation 4 with $a = b = 1/2$ and $\phi = 0$, while ASV-DHS generalizes this by allowing ϕ to be estimated from the data. The distinction between ASV with and without nugget is shown in Equation 5. All ASV models use $k = 1$, applying shrinkage to the first-order differences of the latent log-variance process. This choice reflects the empirical observation that volatility in the SV or GARCH-type models typically exhibits clustering rather than gradual changes in slope.

Eight DGPs are considered: DGP 1–3 use SV models with one to three regimes; DGP 4–6 use GARCH models with one to three regimes; DGP 7 features sinusoidal log-variance with random coefficients; and DGP 8 involves piecewise constant log-variance with 3 to 5 random breakpoints. For each DGP, 1,000 sample paths are simulated. Detailed parameterization of the DGPs may be found in Table 1.

Model performance is evaluated using three metrics: Mean Absolute Error (MAE), Empirical Coverage (EC), and Mean Credible Interval Width (MCIW):

$$MAE = \frac{1}{T} \sum_{t=1}^T |\sigma_t - \hat{\sigma}_t|, \quad EC = \frac{1}{T} \sum_{t=1}^T \mathbb{1}_{(\hat{\sigma}_{t,0.05}, \hat{\sigma}_{t,0.95})}(\sigma_t), \quad MCIW = \frac{1}{T} \sum_{t=1}^T (\hat{\sigma}_{t,0.95} - \hat{\sigma}_{t,0.05}).$$

The MAE measures the accuracy of the volatility estimate by calculating the average absolute difference between the true volatility σ_t and the model's estimate $\hat{\sigma}_t$. For Frequentist methods, the point estimate is based on its maximum likelihood estimate, while it is the posterior mean for the Bayesian methods. The EC assesses the reliability of each model's uncertainty quantification by calculating the proportion of the true volatility falling within the model's 90% credible interval. Finally, the MCIW evaluates the precision of the

uncertainty quantification, where a narrower credible interval represents a higher level of precision.

All models are implemented in **R** language [R Core Team, 2013]. Specifically, the SV model is implemented via **stochvol** package [Kastner, 2016], MSSV2 as specified in Hamilton [1989] and RWSV are implemented by the authors as no readily available packages in **R** exist. GARCH(1,1) is fitted via **fGarch** package [Wuertz et al., 2023], and MSGARCH2 is fitted via **MSGARCH** package [Ardia et al., 2019]. For fitting RWSV-BL, **dsp** package by Kowal et al. [2019] and **genlasso** package by Arnold and Tibshirani [2022] are used. **dsp** package by Kowal et al. [2019] is expanded by the authors to implement ASV. For Bayesian models, 5,000 posterior samples are generated after 20,000 burn-ins for each sample path.

4.2 Results

As shown in Table 2 and Figure 3, the proposed ASV models consistently outperform or match the true models in DGPs with large volatility shifts, including DGPs 2, 3, 5, 6, and 8. In DGP 2, their MAE is only marginally higher than that of MSSV2, and in DGP 5, even slightly lower than that of MSGARCH2, both of which are correctly specified for those settings. Notable differences are found in DGPs 3, 6, and 8. In DGP 3, the average MAE of ASV models is 0.24 (sd = 0.07), compared to 0.46 (sd = 0.15) for the next best model, RWSV-BL, leading to 44% reduction. Similar differences are observed in DGPs 5 and 6. Such results underscore ASV’s ability in capturing abrupt structural changes.

ASV models also perform reasonably well in scenarios where the underlying volatility is stationary or smoothly varying, as in DGPs 1, 4, and 7. SV and GARCH achieve the lowest average MAEs in DGPs 1 and 4 due to perfect specification; ASV models perform similarly to other misspecified models. In DGP 7, where volatility evolves smoothly

		DGP ID							
True Model		1	2	3	4	5	6	7	8
		SV (1 regime)	SV (2 regimes)	SV (3 regimes)	GARCH (1 regime)	GARCH (2 regimes)	GARCH (3 regimes)	Sinusoidal	Piecewise
SV	0.4183 (0.0195)	4.3355 (0.9853)	0.4948 (0.1645)	0.1641 (0.0212)	1.2965 (0.2978)	1.2804 (0.3159)	1.1831 (0.9398)	2.0796 (0.1713)	
MSSV2	0.6288 (1.6236)	1.0265 (0.2822)	0.4904 (0.1676)	0.3034 (1.1001)	2.6322 (2.9965)	3.1646 (3.4242)	2.6815 (2.5832)	2.019 (0.1632)	
GARCH	0.4297 (0.0227)	5.8768 (0.8117)	0.9623 (0.2776)	0.0421 (0.0181)	2.0226 (0.456)	1.8237 (0.437)	2.7572 (2.2338)	4.1509 (0.3525)	
MSGARCH2	0.4334 (0.0318)	5.9983 (1.6226)	1.1078 (1.2224)	0.0577 (0.0206)	0.9559 (0.1991)	1.247 (0.26)	2.1427 (1.6771)	2.7224 (0.7748)	
MAE	RWSV	0.4745 (0.0309)	4.2692 (0.9614)	0.4875 (0.161)	0.1704 (0.0199)	1.2744 (0.2905)	1.2576 (0.309)	1.1668 (0.925)	2.0301 (0.1692)
	RWSV-BL	1.0103 (0.0597)	3.4705 (0.7682)	0.4641 (0.152)	0.2811 (0.0311)	1.4004 (0.3371)	1.4543 (0.3761)	1.42 (1.0283)	1.9933 (0.1658)
ASV-HS	0.4487 (0.0304)	1.4681 (0.3292)	0.2367 (0.0749)	0.1766 (0.0208)	0.967 (0.2199)	1.0518 (0.2559)	0.9348 (0.7365)	1.2409 (0.1392)	
ASV-DHS	0.4517 (0.0313)	1.4892 (0.3192)	0.2369 (0.0725)	0.1777 (0.0212)	0.9462 (0.2124)	1.0336 (0.2535)	0.9426 (0.7442)	1.2209 (0.1385)	
ASV-HS-N	0.4437 (0.0292)	1.4623 (0.3275)	0.236 (0.0746)	0.1776 (0.0209)	0.9754 (0.2228)	1.0617 (0.2558)	0.9358 (0.7373)	1.2449 (0.1386)	
ASV-DHS-N	0.4477 (0.0304)	1.4892 (0.3205)	0.237 (0.0725)	0.1783 (0.0212)	0.9537 (0.2146)	1.0414 (0.2558)	0.9427 (0.7423)	1.2242 (0.1382)	
SV	1.7151 (0.4996)	23.9914 (5.5341)	2.6681 (0.943)	0.8261 (0.0985)	6.9493 (1.6761)	6.9645 (1.7686)	6.9224 (5.4048)	10.5937 (0.8248)	
MSSV2	1.6856 (0.8774)	6.1165 (2.2849)	2.9168 (0.9828)	1.2632 (1.4566)	8.1412 (1.9785)	8.4577 (2.134)	7.9837 (4.4592)	11.0375 (0.8436)	
GARCH	-	-	-	-	-	-	-	-	
MSGARCH2	-	-	-	-	-	-	-	-	
RWSV	1.4682 (0.0678)	23.6249 (5.4109)	2.6127 (0.9215)	0.707 (0.1036)	6.7469 (1.6199)	6.7313 (1.7063)	6.801 (5.3228)	10.0901 (0.7914)	
RWSV-BL	5.8851 (0.178)	19.7094 (4.3992)	2.5829 (0.8688)	1.6936 (0.1421)	7.9766 (1.9155)	8.4779 (2.1574)	8.4593 (6.0041)	10.6267 (0.7472)	
ASV-HS	1.0195 (0.1345)	6.4652 (1.3967)	1.0349 (0.3281)	0.6527 (0.1079)	4.1906 (0.9517)	4.0595 (1.0181)	4.2954 (3.2816)	6.4435 (0.4201)	
ASV-DHS	1.0711 (0.1338)	6.5254 (1.3109)	1.026 (0.3029)	0.6442 (0.1047)	4.0214 (0.8943)	3.9701 (0.9812)	4.3191 (3.3025)	6.3782 (0.4163)	
ASV-HS-N	1.7522 (0.3342)	7.0025 (1.4975)	1.1211 (0.3554)	0.7136 (0.1034)	4.4482 (1.0088)	4.4818 (1.0088)	4.6034 (3.4542)	6.6306 (0.4303)	
ASV-DHS-N	1.7898 (0.3295)	7.1332 (1.431)	1.1215 (0.3332)	0.7127 (0.1017)	4.2736 (0.9445)	4.3395 (1.0468)	4.6343 (3.4943)	6.5572 (0.4303)	
SV	0.8655 (0.0968)	0.9159 (0.0093)	0.9177 (0.0104)	0.9621 (0.0131)	0.9296 (0.0116)	0.9327 (0.0121)	0.9764 (0.0114)	0.9091 (0.0107)	
MSSV2	0.8348 (0.1264)	0.9589 (0.0368)	0.939 (0.0113)	0.9839 (0.0176)	0.9451 (0.0105)	0.9514 (0.0103)	0.9757 (0.0085)	0.9173 (0.0101)	
GARCH	-	-	-	-	-	-	-	-	
MSGARCH2	-	-	-	-	-	-	-	-	
RWSV	0.7779 (0.0276)	0.9144 (0.0094)	0.9148 (0.0107)	0.9081 (0.0248)	0.9252 (0.0123)	0.9274 (0.0113)	0.9758 (0.0118)	0.8973 (0.0112)	
RWSV-BL	0.9718 (0.0098)	0.9549 (0.0092)	0.9515 (0.0101)	0.972 (0.01)	0.9557 (0.0099)	0.96 (0.0097)	0.975 (0.0093)	0.9422 (0.0107)	
ASV-HS	0.6221 (0.0435)	0.9106 (0.0265)	0.9094 (0.0263)	0.8678 (0.0468)	0.9194 (0.0456)	0.8721 (0.0582)	0.9275 (0.0295)	0.9569 (0.0168)	
ASV-DHS	0.6426 (0.041)	0.9009 (0.0281)	0.8973 (0.0278)	0.8584 (0.045)	0.9186 (0.0387)	0.8765 (0.0519)	0.9264 (0.0296)	0.9583 (0.017)	
ASV-HS-N	0.8701 (0.0577)	0.9388 (0.0206)	0.9371 (0.0205)	0.9014 (0.0335)	0.9317 (0.0374)	0.8996 (0.0448)	0.9498 (0.0245)	0.9614 (0.0156)	
ASV-DHS-N	0.8753 (0.0539)	0.9355 (0.0217)	0.9329 (0.0219)	0.8988 (0.0314)	0.9338 (0.032)	0.9035 (0.0415)	0.9494 (0.0245)	0.963 (0.0155)	

Table 2: Model performance under each data-generating process (DGP 1–8), evaluated using: MAE (mean absolute error), MCIW (mean 90% credible interval width), and EC (empirical 90% coverage). Standard deviations are shown in parentheses. For each DGP, the two models with the lowest average MAE and the four models with the narrowest average MCIW are highlighted in bold.

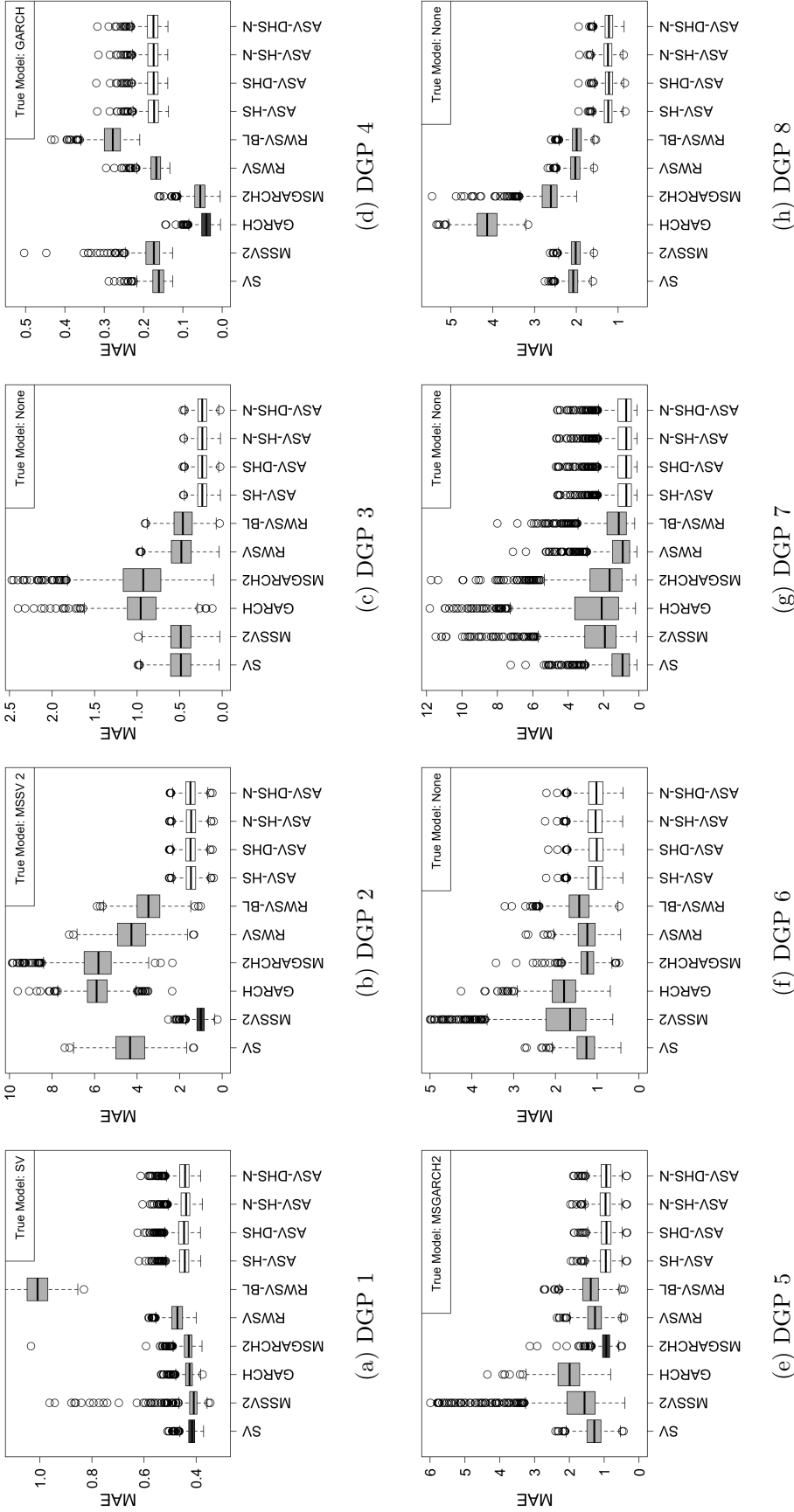


Figure 3: Box plots of Mean Absolute Error (MAE) across 1,000 sample paths comparing 1,000 sample paths comparing Stochastic Volatility (SV), Markov-Switching Stochastic Volatility with 2 Regimes (MSSV2), Generalized AutoRegressive Conditional Heteroskedasticity (GARCH), Markov-Switching GARCH with 2 Regimes (MSGARCH2), Random Walk SV with Inverse Gamma Prior (RWSV), Random Walk SV with Bayesian LASSO (RWSV-BL), Adaptive SV with the horseshoe prior (ASV-HS), and ASV with dynamic horseshoe prior (ASV-DHS). Perfectly specified models, drawn in black, are SV and MSSV2 for DGP 1 and 2 and GARCH and MSGARCH2 for DGP 4 and 5. All models are misspecified for DGP 3 and 6.

without abrupt shifts, ASV outperforms all models including SV and RWSV. This suggests that although ASV is designed to capture abrupt structural changes, it still maintains competitive performance in settings that favor smooth or mean-reverting dynamics.

Also, the simulation study highlights the limitations of HMS models, MSSV2 and MS-GARCH2, which rely on a fixed number of latent regimes. These models perform poorly when the assumed regime structure does not align with the data. Notably, they perform worse than their single-regime counterparts SV and GARCH in scenarios with stationary volatility (DGPs 1 and 4). Their performance also deteriorates when the number discrete levels are more than 2 (DGPs 3, 6, and 8). Even in DGP 7, where volatility evolves smoothly without abrupt changes, the discrete regime-switching assumption introduces artificial segmentation, leading to subpar performance. In contrast, ASV models adaptively estimate volatility using global-local shrinkage, flexibly adjusting to a wide range of structural patterns without assuming a fixed number of regimes.

The second and third row of Table 2 presents the ECs and the MCIWs of the 90% credible intervals of the eight Bayesian methods in the simulation study: SV, MSSV2, RWSV, RWSV-BL and 4 variants of ASV. ASV-HS and ASV-DHS achieve nominal 90% coverage in all DGPs except in DGPs 1 and 4. In DGP 1, they exhibit substantial undercoverage, with empirical coverage dropping to 63%, and in DGP 4, mild undercoverage at 86%. This is likely due to the models' assumption of nonstationarity, which conflicts with the stationary assumption of the DGP. ASV-HS-N and ASV-DHS-N address the undercoverage problem by introducing a nugget effect, achieving correct nominal coverage across all 8 DGPs. In addition, their credible intervals are the narrowest across all eight DGPs aside from their non-nugget counter parts, indicating both precise and robust uncertainty quantification.

The key structural difference between ASV-DHS and ASV-HS is the presence of an

autoregressive shrinkage parameter ϕ in ASV-DHS, which governs the temporal evolution of the local scale parameters. Despite this, they exhibit similar performance across DGPs 1 through 7. This is expected: in DGPs 1, 4, and 7, changes in volatility are gradual. In DGPs 2, 3, 5, and 6, abrupt changes occur but are highly persistent with the transition probability between different states of 2% for DGPs 2 and 5, and only 1% for DGPs 3 and 6, resulting in relatively few shifts. In DGP 8 features frequent and periodic volatility changes. In this setting, ASV-DHS consistently achieves smaller MAEs than ASV-HS. Although the average improvement is modest (0.021), it is consistent across 1,000 replicates, indicating that dynamic shrinkage offers better local adaptivity when volatility shifts are both abrupt and recurrent.

5 Empirical Study

We continue our analysis of the datasets introduced in Section 1 and estimate the log-variance using four methods: SV and MSSV2, which serve as established baselines, and ASV-DHS and ASV-DHS-N, our proposed models. For the ASV models, we set $k = 1$ to reflect the presence of abrupt changes observed in Figure 1. In the S&P 500 dataset (Figures 4a to 4d), all models detect major volatility spikes in 2009 and 2020, corresponding to the global financial crisis and the COVID-19 pandemic. Moderate increases are also identified around 2001 (9/11), 2011 (European debt crisis), and 2018 (U.S. government shutdowns). ASV-DHS and ASV-DHS-N provide smoother and more stable estimates compared to SV and MSSV2, particularly during low-volatility periods.

For both the electricity (Figures 4e to 4h), and bike rental datasets (Figures 4i to 4l), all methods capture strong seasonal patterns in volatility, with elevated uncertainty coinciding with periods of peak activity. In the electricity dataset, this corresponds to high-demand

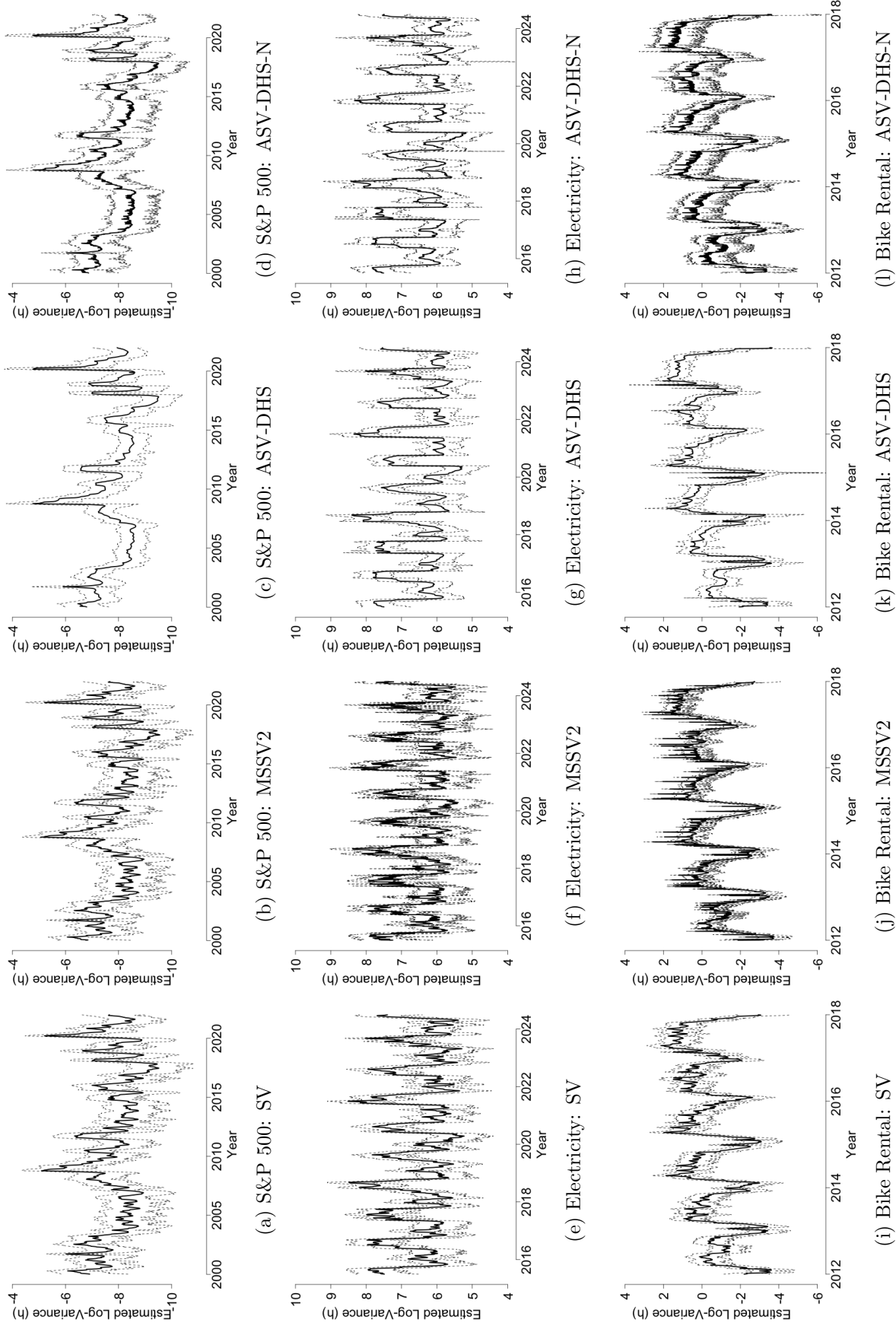


Figure 4: Estimated log-variance from four methods, Stochastic Volatility (SV), Markov-Switching SV with two regimes (MSSV2), Adaptive Stochastic Volatility with the dynamic horseshoe prior (ASV-DHS), and ASV-DHS with a nugget effect, applied to three datasets: weekly S&P 500 log returns, daily electricity demand, and daily bike rental counts.

months, while in the bike rental dataset, volatility increases during summer.

Dataset	Metric	SV	MSSV2	ASV-DHS	ASV-DHS-N
S&P 500	Mean	0.0739	0.0792	0.037	0.0799
	Kurtosis	0.9105	0.7348	52.3562	11.5863
	CP	0	0	9	3
Electricity	Mean	0.0307	0.0600	0.0176	0.0213
	Kurtosis	0.1691	7.5788	65.4116	68.4159
	CP	0	4	16	20
Bike	Mean	0.0616	0.143	0.0456	0.1331
	Kurtosis	0.1989	13.3789	90.7971	5.6332
	CP	0	3	10	2

Table 3: Summary statistics for each dataset and model: (1) the mean and (2) kurtosis of the estimated log-variance increments $|\Delta\hat{h}_t|$ and (3) the total number of flagged change points (CP). CP are computed as $\sum_{t=2}^T \mathbb{1}\{|\Delta\hat{h}_t| > \delta\}$, where $\delta := 5 \times \text{sd}(\Delta\hat{h}_t)$.

Table 3 presents summary metrics of the estimated log-variance increments $|\Delta\hat{h}_t|$ across the three empirical datasets. These metrics, mean, kurtosis, and the number of flagged change points (CP), offer insight into the smoothness, tail behavior, and local adaptivity. ASV-DHS consistently produces the lowest mean, indicating highly smooth volatility trajectories. At the same time, it shows extremely high kurtosis and the highest number of flagged change points, suggesting heavy-tailed behavior in the increments and strong local adaptivity to sudden structural shifts. These properties highlight the model's tendency to promote overall smoothness while remaining responsive to large isolated changes.

The smoothness of ASV-DHS-N adapts to the structure of the data. In the electricity dataset, where the volatility is characterized by extended periods of small changes punctuated by occasional abrupt shifts, the mean in Table 3 under ASV-DHS-N is similar to that of ASV-HS. In contrast, for the bike rental and S&P 500 datasets, which exhibit more unpredictable changes in volatility, the smoothness profile of ASV-DHS-N resembles that of MSSV2. The kurtosis remains substantially higher than that of SV and MSSV2, preserving the model's ability to capture heavy-tailed behavior. The CP is also notably higher than

that of SV, reflecting greater local adaptivity, though still lower than that of ASV-DHS.

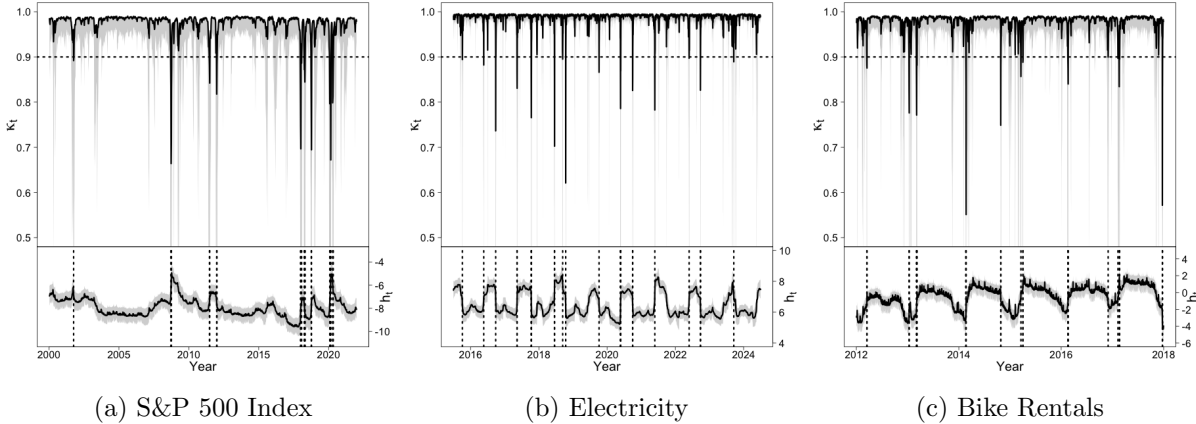


Figure 5: Comparison of the posterior means of the shrinkage parameter $\kappa_t := 1/(1 + \exp\{v_t\})$, where $v_t = \log(\text{Var}(\Delta h_t))$, and the log-variance parameter h_t , estimated using ASV-DHS-N on the S&P 500, electricity demand, and bike rental datasets. The shaded regions represent the 95% and centered 90% credible intervals for κ_t and h_t , respectively. Vertical lines indicate dates where the expected κ_t falls below 0.9.

Another defining feature of ASV is its ability to localize the timing of large variations in volatility through the shrinkage parameter $\kappa_t := \frac{1}{1+\exp(v_t)}$. κ_t close to 0 corresponds to high variability in the latent volatility increments Δh_t , indicating periods of substantial changes in h_t , while a κ_t near 1 suggests strong shrinkage and minimal change. Thus κ_t serves as an interpretable signal for identifying the timing of structural shifts in volatility.

In Figure 5, we highlight time points where the posterior mean of κ_t drops below 0.9, marking potential locations of abrupt volatility changes. For the S&P 500 index (Figure 5a), this includes notable episodes explored in earlier paragraph, such as the 2008 financial crisis, the 2011 European debt crisis, and the COVID-19 shock in early 2020. In Figure 5b, electricity usage spikes in volatility around late spring and early fall, periods that typically mark transitions in heating or cooling demand, reflecting changing usage patterns driven by weather fluctuations. Figure 5b shows a similar pattern with volatility spikes in bike rental counts occurring near the start of spring such as late February and March and near the end-of-year holiday season in December and January.

6 Trend Filtering Jointly in Mean and Variance

The Bayesian Trend Filter with DSP (BTF-DSP) by Kowal et al. [2019] provides a smooth and locally adaptive estimate of the mean of a time series. As an extension, we propose the Bayesian Trend Filter with ASV (BTF-ASV), thereby allowing locally adaptive estimates of both the mean $\{\beta_t\}_{t=1}^T$, and the log variance process $\{h_t\}_{t=1}^T$ simultaneously:

$$\begin{aligned} y_t &= \beta_t + \exp\{h_t/2\}\epsilon_t \quad [\epsilon_t] \stackrel{iid}{\sim} N(0, 1), \\ [\Delta^{k_\beta} \beta_t | \sigma_{\beta,t}^2] &\sim N(0, \sigma_{\beta,t}^2) \quad [\log(\sigma_{\beta,t}^2) | \mu_\beta, \phi_\beta] \sim DSP(a_\beta, b_\beta, \mu_\beta, \phi_\beta), \\ [\Delta^{k_h} h_t | \sigma_{h,t}^2] &\sim N(0, \sigma_{h,t}^2) \quad [\log(\sigma_{h,t}^2) | \mu_h, \phi_h] \sim DSP(a_h, b_h, \mu_h, \phi_h). \end{aligned} \quad (6)$$

We impose two conditionally independent priors on the k th-order differences of β_t and h_t . The model distinguishes changes in the mean from changes in volatility through its structural formulation: β_t enters the likelihood additively, while h_t governs the multiplicative noise scale. This separation ensures that fluctuations in the variance do not influence the location of the distribution. Below, we show that the model is identifiable in the sense that the evolution variance terms, $\sigma_{\beta,t}^2$ and $\sigma_{h,t}^2$, are uniquely determined by the observed data.

Theorem 4. *The following model is identifiable:*

$$\begin{aligned} y_t &= \beta_t + \exp\{h_t/2\}\epsilon_t \quad [\epsilon_t] \stackrel{iid}{\sim} N(0, 1), \\ [\Delta^k \beta_t | \sigma_{\mu,t}^2] &\sim N(0, \sigma_{\mu,t}^2) \quad [\Delta^k h_t | \sigma_{h,t}^2] \sim N(0, \sigma_{h,t}^2). \end{aligned}$$

Proof. For contradiction, fix two distinct parameter vectors $\boldsymbol{\theta} := (\boldsymbol{\beta}, \mathbf{h}, \boldsymbol{\lambda}_\mu, \boldsymbol{\lambda}_h)$ and $\boldsymbol{\theta}^* := (\boldsymbol{\beta}^*, \mathbf{h}^*, \boldsymbol{\lambda}_\mu^*, \boldsymbol{\lambda}_h^*)$ such that $\boldsymbol{\theta} \neq \boldsymbol{\theta}^*$ and $f(y|\boldsymbol{\theta}) = f(y|\boldsymbol{\theta}^*)$. Indeed, $\text{Var}(y|\boldsymbol{\theta}) = \text{Var}(y|\boldsymbol{\theta}^*)$. This covariance equality necessarily forces $\boldsymbol{\theta} = \boldsymbol{\theta}^*$, leading to contradiction. Detailed proof

is shown in Appendix A. □

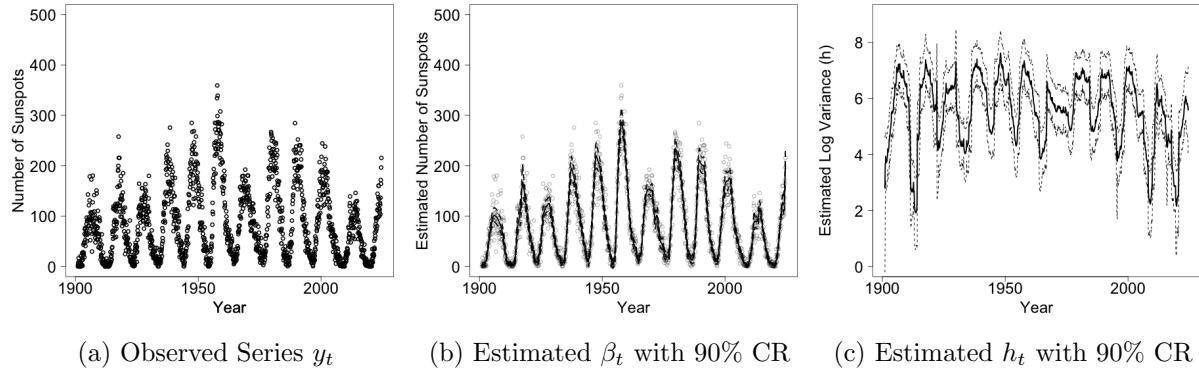


Figure 6: Monthly mean total sunspot number, the average value of the daily total sunspot numbers over all days of each calendar month, from Jan. 1901 to Aug. 2024 is illustrated in 6a. The Bayesian Trend Filter with Adaptive Stochastic Volatility (BTF-ASV) is used to estimate the mean trend β_t and is illustrated in 6b. The estimate of log-variance h_t and its 90% credible intervals is shown in 6c.

BTF-ASV is applied to the sunspot data to estimate both the time varying mean and the volatility. The data consist of monthly mean total sunspot numbers, defined as the average daily total over each calendar month, from January 1901 to August 2024, obtained from SILSO World Data Center [2025]. The number of sunspots exhibits a well-known cyclic pattern associated with the 11-year solar cycle, which reflects periodic fluctuations in solar magnetic activity. This cyclical behavior is clearly visible in the raw observations shown in Figure 6a. The BTF estimate of the mean trend, β_t , shown in Figure 6b, provides a smooth reconstruction of this underlying cycle.

Interestingly, the estimated log-variance (Figure 6c) also follows a cyclical pattern that closely aligns with the mean trend. Periods of increased solar activity are associated with elevated volatility, suggesting that not only does solar activity rise and fall periodically, but the variability around these phases also intensifies. This highlights BTF-ASV's ability to decompose a noisy data into structured patterns in both the mean and variance process, offering a richer understanding of solar dynamics.

7 Conclusion

We propose ASV, a flexible and locally adaptive model for capturing both abrupt and gradual changes in volatility. ASV extends RWSV by incorporating global-local shrinkage priors, specifically DSP by Kowal et al. [2019]. We develop and study multiple variants of ASV, including models with the horseshoe (ASV-HS), dynamic horseshoe (ASV-DHS), and their nugget-augmented counterparts (ASV-HS-N and ASV-DHS-N).

Through extensive simulation studies, we show that ASV-HS-N and ASV-DHS-N consistently achieve low MAE, correct nominal coverage, and narrower credible intervals compared to existing volatility models. Although ASV variants without the nugget term perform similarly in terms of point estimation, they tend to exhibit under-coverage in stationary settings due to their lack of a noise-absorbing layer. Empirical applications demonstrate that ASV models effectively capture large structural changes in volatility while preserving smooth estimates in stable periods. Moreover, the shrinkage parameter κ_t provides a useful diagnostic for further identifying the timing of structural shifts.

Finally, we integrate ASV into the error process of the Bayesian Trend Filter proposed in Kowal et al. [2019], resulting in BTF-ASV. Empirical studies reveal its ability to produce smooth estimates of both time-varying mean and time-varying variance. Future research directions could explore the applications of ASV and BTF-ASV in diverse fields such as finance, environmental science, and epidemiology, leveraging their adaptability in modeling time-series exhibiting complex patterns.

8 Acknowledgement

Financial support from National Science Foundation grants OAC-1940124 and DMS-2114143

is gratefully acknowledged.

9 Supplementary Material

Appendices: A document including detailed proofs on the properties of Dynamic Shrinkage Processes (DSP) in section A. The exact prior distributions and detailed derivations of the full conditional distributions for Gibbs sampling in section B.

References

J. Achcar, R. de Oliveira, and E. Barili. Use of stochastic volatility models in epidemiological data: Application to a dengue time series in são paulo city, brazil. *Journal of Biostatistics and Epidemiology*, 6(1):19–29, Oct. 2020. doi: 10.18502/jbe.v6i1.4755. URL <https://jbe.tums.ac.ir/index.php/jbe/article/view/338>.

D. Ardia, K. Bluteau, K. Boudt, and L. Catania. Forecasting risk with markov-switching garch models: A large-scale performance study. *International Journal of Forecasting*, 34(4):733–747, 2018.

D. Ardia, K. Bluteau, K. Boudt, L. Catania, and D.-A. Trottier. Markov-switching garch models in r: The msgarch package. *Journal of Statistical Software*, 91(4):1–38, 2019. doi: 10.18637/jss.v091.i04.

T. B. Arnold and R. J. Tibshirani. *genlasso: Path Algorithm for Generalized Lasso Problems*, 2022. URL <https://CRAN.R-project.org/package=genlasso>. R package version 1.6.1.

O. Barndorff-Nielsen, J. Kent, and M. Sørensen. Normal variance-mean mixtures and z distributions. *International Statistical Review / Revue Internationale de Statistique*, 50(2):145–159, 1982. ISSN 03067734, 17515823. URL <http://www.jstor.org/stable/1402598>.

L. Bauwens, A. Preminger, and J. V. K. Rombouts. Theory and inference for a markov switching garch model. *The Econometrics Journal*, 13(2):218–244, 2010. ISSN 13684221, 1368423X. URL <http://www.jstor.org/stable/23117467>.

A. Bhadra, J. Datta, N. G. Polson, and B. Willard. The horseshoe+ estimator of ultra-sparse signals, 2015.

C. Bikeshare. Capital bikeshare system data, 2024. URL <https://capitalbikeshare.com/system-data>. Accessed: 2024-06-16.

M. Billio, R. Casarin, and A. Osuntuyi. Efficient gibbs sampling for markov switching garch models. *Computational Statistics & Data Analysis*, 100:37–57, 2016. ISSN 0167-9473. doi: <https://doi.org/10.1016/j.csda.2014.04.011>. URL <https://www.sciencedirect.com/science/article/pii/S0167947314001182>.

T. Bollerslev. Generalized autoregressive conditional heteroskedasticity. *Journal of Econometrics*, 31(3):307–327, 1986. ISSN 0304-4076. doi: [https://doi.org/10.1016/0304-4076\(86\)90063-1](https://doi.org/10.1016/0304-4076(86)90063-1). URL <https://www.sciencedirect.com/science/article/pii/0304407686900631>.

C. Brunetti, C. Scotti, R. S. Mariano, and A. H. Tan. Markov switching garch models of currency turmoil in southeast asia. *Emerging Markets Review*, 9(2):104–128, 2008.

A. Cadonna, S. Frühwirth-Schnatter, and P. Knaus. Triple the gamma – a unifying shrinkage prior for variance and variable selection in sparse state space and tvp models, 2019.

J. Cai. A markov model of switching-regime arch. *Journal of Business & Economic Statistics*, 12(3):309–316, 1994. ISSN 07350015. URL <http://www.jstor.org/stable/1392087>.

C. M. Carvalho, N. G. Polson, and J. G. Scott. The horseshoe estimator for sparse signals. *Biometrika*, 97(2):465–480, 2010. ISSN 00063444, 14643510. URL <http://www.jstor.org/stable/25734098>.

R. Y. Chou. Volatility persistence and stock valuations: Some empirical evidence using garch. *Journal of Applied Econometrics*, 3(4):279–294, 1988. ISSN 08837252, 10991255. URL <http://www.jstor.org/stable/2096644>.

U. E. I. A. EIA. New york independent system operator electricity demand data, 2024. URL https://www.eia.gov/electricity/gridmonitor/dashboard/electric_overview/regional/REG-NY. Accessed: 2024-06-16.

R. F. Engle. Autoregressive conditional heteroscedasticity with estimates of the variance of united kingdom inflation. *Econometrica*, 50(4):987–1007, 1982. ISSN 00129682, 14680262. URL <http://www.jstor.org/stable/1912773>.

M. Figueiredo. Adaptive sparseness for supervised learning. *IEEE Transactions on Pattern Analysis and Machine Intelligence*, 25(9):1150–1159, 2003. doi: 10.1109/TPAMI.2003.1227989.

Y. Finance. Historical data, April 2025. URL <https://finance.yahoo.com/quote/^GSPC/history>. Data accessed from Yahoo Finance on April 02, 2025. Data includes historical stock prices, dividends, and splits.

K. French, G. Schwert, and R. Stambaugh. Expected stock returns and volatility. *Journal of Financial Economics*, 19(1):3–29, 1987. URL <https://EconPapers.repec.org/RePEc:eee:jfinec:v:19:y:1987:i:1:p:3-29>.

S. F. Gray. Modeling the conditional distribution of interest rates as a regime-switching process. *Journal of Financial Economics*, 42(1):27–62, September 1996a. URL <https://ideas.repec.org/a/eee/jfinec/v42y1996i1p27-62.html>.

S. F. Gray. Modeling the conditional distribution of interest rates as a regime-switching process. *Journal of Financial Economics*, 42(1):27–62, 1996b. ISSN 0304-405X. doi: [https://doi.org/10.1016/0304-405X\(96\)00875-6](https://doi.org/10.1016/0304-405X(96)00875-6). URL <https://www.sciencedirect.com/science/article/pii/0304405X96008756>.

J. E. Griffin and P. J. Brown. Alternative prior distributions for variable selection with very many more variables than observations. Technical Report 05-20, University of Warwick, Centre for Research in Statistical Methodology, 2005. URL <https://wrap.warwick.ac.uk/id/eprint/35585/>.

J. D. Hamilton. A new approach to the economic analysis of nonstationary time series and the business cycle. *Econometrica*, 57(2):357–384, 1989. ISSN 00129682, 14680262. URL <http://www.jstor.org/stable/1912559>.

J. D. Hamilton and R. Susmel. Autoregressive conditional heteroskedasticity and changes in regime. *Journal of Econometrics*, 64(1):307–333, 1994. ISSN 0304-4076. doi: [https://doi.org/10.1016/0304-4076\(94\)90067-1](https://doi.org/10.1016/0304-4076(94)90067-1). URL <https://www.sciencedirect.com/science/article/pii/0304407694900671>.

A. Harvey, E. Ruiz, and N. Shephard. Multivariate stochastic variance models. *The Review of Economic Studies*, 61(2):247–264, 04 1994. ISSN 0034-6527. doi: 10.2307/2297980. URL <https://doi.org/10.2307/2297980>.

R. J. Hodrick and E. C. Prescott. Postwar u.s. business cycles: An empirical investigation. *Journal of Money, Credit and Banking*, 29(1):1–16, 1997. ISSN 00222879, 15384616. URL <http://www.jstor.org/stable/2953682>.

J. Hull and A. White. The pricing of options on assets with stochastic volatilities. *The Journal of Finance*, 42(2):281–300, 1987. doi: <https://doi.org/10.1111/j.1540-6261.1987.tb02568.x>. URL <https://onlinelibrary.wiley.com/doi/abs/10.1111/j.1540-6261.1987.tb02568.x>.

S. Hwang, S. E. Satchell, and P. L. V. Pereira. How Persistent is Volatility? An Answer with Stochastic Volatility Models with Markov Regime Switching State Equations. Econometric Society 2004 Latin American Meetings 198, Econometric Society, Aug. 2004. URL <https://ideas.repec.org/p/ecm/latm04/198.html>.

E. Jacquier, N. G. Polson, and P. E. Rossi. Bayesian analysis of stochastic volatility models. *Journal of Business & Economic Statistics*, 12(4):371–389, 1994. ISSN 07350015. URL <http://www.jstor.org/stable/1392199>.

G. Kastner. Dealing with stochastic volatility in time series using the R package stochvol. *Journal of Statistical Software*, 69(5):1–30, 2016. doi: 10.18637/jss.v069.i05.

G. Kastner and S. Frühwirth-Schnatter. Ancillarity-sufficiency interweaving strategy (ASIS) for boosting MCMC estimation of stochastic volatility models. *Computational Statistics & Data Analysis*, 76:408–423, aug 2014. doi: 10.1016/j.csda.2013.01.002. URL <https://doi.org/10.1016%2Fj.csda.2013.01.002>.

S. Kim, N. Shephard, and S. Chib. Stochastic volatility: Likelihood inference and comparison with arch models. *The Review of Economic Studies*, 65(3):361–393, 1998. ISSN 00346527, 1467937X. URL <http://www.jstor.org/stable/2566931>.

S.-J. Kim, K. Koh, S. Boyd, and D. Gorinevsky. l_1 trend filtering. *SIAM Rev.*, 51(2):339–360, 2009. ISSN 0036-1445,1095-7200. doi: 10.1137/070690274. URL <https://doi.org/10.1137/070690274>.

P. Kostoulas, E. Meletis, K. Pateras, P. Eusebi, T. Kostoulas, L. Furuya-Kanamori, N. Speybroeck, M. Denwood, S. Doi, C. Althaus, C. Kirkeby, P. Rohani, N. Dhand, J. Peñalvo, L. Thabane, B. m. Slimane, H. Sharifi, and S. Walter. The epidemic volatility index, a novel early warning tool for identifying new waves in an epidemic. *Scientific Reports*, 11:23775, 12 2021. doi: 10.1038/s41598-021-02622-3.

D. R. Kowal, D. S. Matteson, and D. Ruppert. Dynamic Shrinkage Processes. *Journal of the Royal Statistical Society Series B: Statistical Methodology*, 81(4):781–804, 05 2019. ISSN 1369-7412. doi: 10.1111/rssb.12325. URL <https://doi.org/10.1111/rssb.12325>.

J. Ma, F. Xu, K. Huang, and R. Huang. Gnar-garch model and its application in feature extraction for rolling bearing fault diagnosis. *Mechanical Systems and Signal Processing*, 93:175–203, 2017.

S. Mehdizadeh, J. Behmanesh, and K. Khalili. A comparison of monthly precipitation point estimates at 6 locations in iran using integration of soft computing methods and garch time series model. *Journal of Hydrology*, 554:721–742, 2017. ISSN 0022-1694. doi: <https://doi.org/10.1016/j.jhydrol.2017.09.056>. URL <https://www.sciencedirect.com/science/article/pii/S0022169417306601>.

A. Melino and S. M. Turnbull. Pricing foreign currency options with stochastic volatility. *Journal of Econometrics*, 45(1-2):239–265, 1990. URL <https://EconPapers.repec.org/RePEc:eee:econom:v:45:y:1990:i:1-2:p:239-265>.

R. Modarres and T. B. Ouarda. Modeling the relationship between climate oscillations and drought by a multivariate garch model. *Water Resources Research*, 50(1):601–618, 2014.

R. M. Neal. Slice sampling. *The Annals of Statistics*, 31(3):705 – 767, 2003. doi: 10.1214/aos/1056562461. URL <https://doi.org/10.1214/aos/1056562461>.

H. Nishino and K. Kakamu. A random walk stochastic volatility model for income inequality. *Japan and the World Economy*, 36:21–28, 2015. ISSN 0922-1425. doi: <https://doi.org/10.1016/j.japwor.2015.06.003>. URL <https://www.sciencedirect.com/science/article/pii/S0922142515000328>.

Y. Omori, S. Chib, N. Shephard, and J. Nakajima. Stochastic volatility with leverage: Fast and efficient likelihood inference. *Journal of Econometrics*, 140(2):425–449, 2007. ISSN 0304-4076. doi: <https://doi.org/10.1016/j.jeconom.2006.07.008>. URL <https://www.sciencedirect.com/science/article/pii/S0304407606001436>.

M. Otache. Conditional heteroscedasticity in streamflow process: Paradox or reality? *Open Journal of Modern Hydrology*, 02:79–90, 01 2012. doi: 10.4236/ojmh.2012.24010.

T. Park and G. Casella. The bayesian lasso. *Journal of the American Statistical Association*, 103(482):681–686, 2008. doi: 10.1198/016214508000000337. URL <https://doi.org/10.1198/016214508000000337>.

H. T. Pham and B.-S. Yang. Estimation and forecasting of machine health condition using arma/garch model. *Mechanical systems and signal processing*, 24(2):546–558, 2010.

N. G. Polson, J. G. Scott, and J. Windle. Bayesian inference for logistic models using polya-gamma latent variables, 2013.

S.-H. Poon and S. J. Taylor. Stock returns and volatility: An empirical study of the uk stock market. *Journal of Banking & Finance*, 16(1):37–59, 1992. ISSN 0378-4266. doi: [https://doi.org/10.1016/0378-4266\(92\)90077-D](https://doi.org/10.1016/0378-4266(92)90077-D). URL <https://www.sciencedirect.com/science/article/pii/037842669290077D>. Special Issue on European Capital Markets.

R Core Team. *R: A Language and Environment for Statistical Computing*. R Foundation for Statistical Computing, Vienna, Austria, 2013. URL <http://www.R-project.org/>.

E. A. Roualdes. Bayesian trend filtering, 2015. URL <https://arxiv.org/abs/1505.07710>.

E. Ruiz. Quasi-maximum likelihood estimation of stochastic volatility models. *Journal of Econometrics*, 63(1):289–306, 1994. ISSN 0304-4076. doi: [https://doi.org/10.1016/0304-4076\(93\)01569-8](https://doi.org/10.1016/0304-4076(93)01569-8). URL <https://www.sciencedirect.com/science/article/pii/0304407693015698>.

J. A. Ryan and J. M. Ulrich. *quantmod: Quantitative Financial Modelling Framework*, 2024. URL <https://CRAN.R-project.org/package=quantmod>. R package version 0.4.26.

R. R. Sarkar and C. Chatterjee. Application of different time series models on epidemiological data-comparison and predictions for malaria prevalence. *SM J. Biom. Biostat*, 2(4):1022, 2017.

T. L. J. Schafer and D. S. Matteson. Locally adaptive shrinkage priors for trends and breaks in count time series. *Technometrics*, 0(ja):1–16, 2024. doi: 10.1080/00401706.2024.2407316. URL <https://doi.org/10.1080/00401706.2024.2407316>.

SILSO World Data Center. International sunspot number monthly bulletin and data. <https://www.sidc.be/SILSO/infosnmtot>, 2025. Royal Observatory of Belgium, Brussels. Accessed: 2025-01-01.

M. K. So, K. Lam, and W. Li. An Empirical Study of Volatility in Seven Southeast Asian Stock Markets Using ARV Models. *Journal of Business Finance & Accounting*, 24(2):261–276, March 1997. doi: 10.1111/1468-5957.00104. URL <https://ideas.repec.org/a/bla/jbfac/v24y1997i2p261-276.html>.

M. K. P. So, K. Lam, and W. K. Li. A stochastic volatility model with markov switching. *Journal of Business & Economic Statistics*, 16(2):244–253, 1998. ISSN 07350015. URL <http://www.jstor.org/stable/1392580>.

W. E. Strawderman. Proper bayes minimax estimators of the multivariate normal mean. *The Annals of Mathematical Statistics*, 42(1):385–388, 1971.

F. Su and L. Wang. Conditional volatility persistence and realized volatility asymmetry: Evidence from the chinese stock markets. *Emerging Markets Finance and Trade*, 56(14):3252–3269, 2020. doi: 10.1080/1540496X.2019.1574566. URL <https://doi.org/10.1080/1540496X.2019.1574566>.

S. J. Taylor. *Modelling Financial Time Series*. G - Reference,Information and Interdisciplinary Subjects Series. World Scientific, 2008. ISBN 9789812770844. URL <https://books.google.com/books?id=KQ5pDQAAQBAJ>.

R. Tibshirani. Regression shrinkage and selection via the lasso. *Journal of the Royal Statistical Society. Series B (Methodological)*, 58(1):267–288, 1996. ISSN 00359246. URL <http://www.jstor.org/stable/2346178>.

R. J. Tibshirani. Adaptive piecewise polynomial estimation via trend filtering. *The Annals of Statistics*, 42(1), Feb. 2014. ISSN 0090-5364. doi: 10.1214/13-aos1189. URL <http://dx.doi.org/10.1214/13-AOS1189>.

M. K. Tippett. Changing volatility of us annual tornado reports. *Geophysical Research Letters*, 41(19):6956–6961, 2014.

H. Wang, S. Song, G. Zhang, O. O. Ayantobo, and T. Guo. Stochastic volatility modeling of daily streamflow time series. *Water Resources Research*, 59(1):e2021WR031662, 2023a. doi: <https://doi.org/10.1029/2021WR031662>. URL <https://agupubs.onlinelibrary.wiley.com/doi/abs/10.1029/2021WR031662> 2021WR031662.

H. Wang, S. Song, G. Zhang, and O. O. Ayantoboc. Predicting daily streamflow with a novel multi-regime switching arima-ms-garch model. *Journal of Hydrology: Regional Studies*, 47:101374, 2023b. ISSN 2214-5818. doi: <https://doi.org/10.1016/j.ejrh.2023.101374>. URL <https://www.sciencedirect.com/science/article/pii/S2214581823000617>.

W. Wang, P. H. A. J. M. Van Gelder, J. K. Vrijling, and J. Ma. Testing and modelling autoregressive conditional heteroskedasticity of streamflow processes. *Nonlinear processes in Geophysics*, 12(1):55–66, 2005.

M. West. On scale mixtures of normal distributions. *Biometrika*, 74(3):646–648, 09 1987. ISSN 0006-3444. doi: 10.1093/biomet/74.3.646. URL <https://doi.org/10.1093/biomet/74.3.646>.

H. Wu, T. L. J. Schafer, and D. S. Matteson. Trend and variance adaptive bayesian changepoint analysis and local outlier scoring. *Journal of Business & Economic Statistics*, 0(0):1–12, 2024a. doi: 10.1080/07350015.2024.2362269. URL <https://doi.org/10.1080/07350015.2024.2362269>.

H. Wu, T. L. J. Schafer, S. Ryan, and D. S. Matteson. Drift vs shift: Decoupling trends and changepoint analysis. *Technometrics*, 0(ja):1–16, 2024b. doi: 10.1080/00401706.2024.2365730. URL <https://doi.org/10.1080/00401706.2024.2365730>.

D. Wuertz, Y. Chalabi, T. Setz, M. Maechler, and G. N. Boshnakov. *fGarch: Rmetrics - Autoregressive Conditional Heteroskedastic Modelling*, 2023. URL <https://www.rmetrics.org>. R package version 4031.90.

A Proofs of Theorems

A.1 Theorem 1

As mentioned, proofs directly follow from Kolmogorov's three series theorem, which state the sufficient and necessary condition for almost sure convergence of infinite sum of random variables. Let $\phi \in (0, 1)$. Due to symmetry of sech function, we only need to prove the case when $0 < \phi < 1$, and the case where $-1 < \phi < 0$, directly follows. For the first condition, let $\epsilon > 0$, and h is some positive integer or 0.

$$\begin{aligned}
P(|z_h| \geq \epsilon) &= 2 \int_{\epsilon}^{\infty} \frac{\exp\{x/(2\phi^h)\}}{\pi\phi^h(1 + \exp\{x/\phi^h\})} dx \\
&= \frac{2}{\pi\phi^h} \int_{\epsilon}^{\infty} \frac{\exp\{x/(2\phi^h)\}}{1 + \exp\{x/\phi^h\}} dx & u = \exp\{x/(2\phi^h)\} \\
&= \frac{4}{\pi} \int_{\epsilon}^{\infty} \frac{1}{1 + u^2} du & 2\phi^h du = \exp\{x/(2\phi^h)\} dx \\
&= \frac{4}{\pi} \arctan(\exp\{x/(2\phi^h)\}) \Big|_{\epsilon}^{\infty} \\
&= 2\left(1 - \frac{2}{\pi} \arctan(\exp\{\epsilon/(2\phi^h)\})\right) \\
&= \frac{4}{\pi} \operatorname{arccotan}(\exp\{\epsilon/(2\phi^h)\}) \\
&\leq \frac{4}{\pi} \operatorname{arccotan}(\exp\{h\}) & \text{if } \epsilon \leq 2h\phi^h
\end{aligned}$$

Since $0 < \phi < 1$, $2h\phi^h$ converges to 0. Also, $2h\phi^h \geq 0$ for $h \geq 0$. For any ϵ , we have h' that satisfies $\epsilon \leq 2h\phi^h$ for $h' \leq h$. Then, fix such h' .

$$\begin{aligned}
\int_{h'}^{\infty} \frac{4}{\pi} \operatorname{arccotan}(\exp\{h\}) dh &< \infty \\
\sum_{h=h'}^{\infty} \frac{4}{\pi} \operatorname{arccotan}(\exp\{\epsilon/(2\phi^h)\}) &\leq \sum_{h=h'}^{\infty} \frac{4}{\pi} \operatorname{arccotan}(\exp\{h\}) < \infty
\end{aligned}$$

Therefore,

$$\sum_{h=0}^{\infty} P(|z_h| \geq \epsilon) = \sum_{h=0}^{\infty} \frac{4}{\pi} \arccotan(\exp\{\epsilon/(2\phi^h)\}) < \infty$$

On the side note, we can also easily see that when $|\phi| > 1$, the sum diverges to ∞ . By Borel-Cantelli lemma, we may conclude that $\sum_{h=0}^{\infty} z_h$ diverges almost surely.

Define $y_h = z_h 1_{\{|z_h| \leq \epsilon\}}$. For the second and the third condition, we need to show that

1) $\sum_{h=0}^{\infty} \mathbb{E}(y_h)$ converges, and 2) $\sum_{h=0}^{\infty} \text{Var}(y_h)$, converges. For the second condition, it suffices to show:

$$\mathbb{E}\left(\sum_{h=0}^{\infty} y_h\right) = \sum_{h=0}^{\infty} \mathbb{E}(y_h) < \infty,$$

which is satisfied by showing $\sum_{h=0}^{\infty} \mathbb{E}(|y_h|) < \infty$ (Fubini). Using Cauchy-Schwartz Inequality:

$$\begin{aligned} \sum_{h=0}^{\infty} \mathbb{E}(|y_h|) &= \sum_{h=0}^{\infty} \mathbb{E}(|z_h 1_{\{|z_h| \leq \epsilon\}}|) \\ &\leq \sum_{h=0}^{\infty} \sqrt{\mathbb{E}(z_h^2) P(|z_h| \leq \epsilon)} \\ &\leq \sum_{h=0}^{\infty} \sqrt{\mathbb{E}(z_h^2)} = \sum_{h=0}^{\infty} \sqrt{\text{Var}(z_h)} = \pi \sum_{h=0}^{\infty} \phi^h = \frac{\pi}{(1-\phi)} < \infty. \end{aligned}$$

The second condition is satisfied. For the third condition, similar logic is applied. First note that:

$$\begin{aligned} \text{Var}\left(\sum_{h=0}^{\infty} y_h\right) &= \mathbb{E}\left(\left(\sum_{h=0}^{\infty} y_h\right)^2\right) + \mathbb{E}\left(\left(\sum_{h=0}^{\infty} y_h\right)\right)^2 \\ &= \mathbb{E}\left(\left(\sum_{h=0}^{\infty} y_h\right)^2\right) + \left(\left(\sum_{h=0}^{\infty} \mathbb{E}(y_h)\right)\right)^2 \\ &= \mathbb{E}\left(\left(\sum_{h=0}^{\infty} y_h\right)^2\right). \end{aligned}$$

And,

$$\begin{aligned}
\lim_{h \rightarrow \infty} \mathbb{E}((\sum_{n=0}^h y_n)^2) &= \lim_{n \rightarrow \infty} \mathbb{E}(\sum_{h=0}^n y_h^2) && \text{(independence)} \\
&= \lim_{n \rightarrow \infty} \sum_{h=0}^n \mathbb{E}(y_h^2) = \sum_{h=0}^{\infty} \mathbb{E}(z_h^2 1_{\{|z_h| \leq \epsilon\}}) \\
&\leq \sum_{h=0}^{\infty} \mathbb{E}(z_h^2) = \frac{\pi^2}{(1 - \phi^2)} < \infty
\end{aligned}$$

Therefore:

$$\text{Var}(\sum_{h=0}^{\infty} y_h) = \sum_{h=0}^{\infty} \text{Var}(y_h) < \infty$$

All three conditions are satisfied.

A.2 Theorem 2

When $\phi = 0.5$, we have the following special case for the MGF,

$$\begin{aligned}
\prod_{h=0}^{\infty} \cos\left(\frac{\pi t}{2^h}\right) &= \prod_{h=0}^{\infty} \frac{\sin\left(\frac{\pi t}{2^{h-1}}\right)}{2 \sin\left(\frac{\pi t}{2^h}\right)} = \lim_{n \rightarrow \infty} \prod_{h=0}^n \frac{\sin\left(\frac{\pi t}{2^{h-1}}\right)}{2 \sin\left(\frac{\pi t}{2^h}\right)} \\
&= \lim_{n \rightarrow \infty} \frac{\sin(2\pi t)}{2^n \sin\left(\frac{\pi t}{2^n}\right)} = \frac{\sin(2\pi t)}{2\pi t}
\end{aligned}$$

We have:

$$\prod_{h=0}^{\infty} \sec\left(\frac{\pi t}{2^h}\right) = \frac{1}{\prod_{h=0}^{\infty} \cos\left(\frac{\pi t}{2^h}\right)} = \frac{2\pi t}{\sin(2\pi t)} = \Gamma(1 - 2t)\Gamma(1 + 2t) = B(1 - 2t, 1 + 2t)$$

$\frac{2\pi t}{\sin(2\pi t)} = \Gamma(1 - 2t)\Gamma(1 + 2t)$ is by the reflection relation. *Logistic*(μ, s) has the the following moment generating function $\exp(-\mu t)B(1 - st, 1 + st)$. Since the moment generating

function uniquely determines the random variable, and by Theorem 2,

$$z_t = \sum_{h=0}^{\infty} z_{t,h} \xrightarrow{a.s} Logistic(0, 2)$$

A.3 Theorem 3

Define $\lambda_t := \exp(v_t)$. We showed that $f(\lambda_t) = \frac{1}{(1+\lambda_t)^2}$. We have:

$$f(\Delta h_t) = \int_0^{\infty} \frac{1}{\sqrt{2\pi\lambda_t^2}} \exp\left(-\frac{\Delta^2 h_t}{2\lambda_t^2}\right) \frac{1}{(1+\lambda_t)^2} d\lambda_t$$

$\forall x > 0$,

$$\frac{1}{2(1+x^2)} \leq \frac{1}{(1+x)^2} \leq \frac{1}{(1+x^2)}.$$

Thus,

$$\begin{aligned} f(\Delta h_t) &\leq \int_0^{\infty} \frac{1}{\sqrt{2\pi\lambda_t^2}} \exp\left(-\frac{\Delta^2 h_t}{2\lambda_t^2}\right) \frac{1}{(1+\lambda_t^2)} d\lambda_t \\ &= \frac{1}{2\sqrt{2\pi}} \int_0^{\infty} \frac{1}{1+u} \exp\left(-\frac{u\Delta^2 h_t}{2}\right) du & u = \frac{1}{\lambda_t^2} \\ &= \frac{1}{2\sqrt{2\pi}} \exp(\Delta^2 h_t/2) E_1(\Delta^2 h_t/2), \end{aligned}$$

where $E_1()$ is the exponential integral function, which satisfies the following upper and lower bound $\forall t > 0$:

$$\frac{\exp(-t)}{2} \log\left(1 + \frac{2}{t}\right) < E_1(t) < \exp(-t) \log\left(1 + \frac{1}{t}\right)$$

Thus,

$$f(\Delta h_t) < \frac{1}{2\sqrt{2\pi}} \log\left(1 + \frac{2}{\Delta^2 h_t}\right)$$

Similarly for the lower bound,

$$f(\Delta h_t) > \frac{1}{8\sqrt{2\pi}} \log \left(1 + \frac{4}{\Delta^2 h_t} \right)$$

The lower and upper bound for $\Delta h_t \neq 0$ is shown. The lower bound clearly approaches infinity as Δh_t approaches 0, which completes the proof.

A.4 Theorem 4

To prove identifiability of the hierarchical model, we need to establish that

1. For any $(\mathbf{h}, \boldsymbol{\beta})$ and $(\mathbf{h}^*, \boldsymbol{\beta}^*)$ in the parameter space, if $f(\mathbf{y}|\mathbf{h}, \boldsymbol{\beta}) = f(\mathbf{y}|\mathbf{h}^*, \boldsymbol{\beta}^*), \forall \mathbf{y} \in \mathcal{Y}$, then $(\mathbf{h}, \boldsymbol{\beta}) = (\mathbf{h}^*, \boldsymbol{\beta}^*)$.
2. For any $(\boldsymbol{\lambda}_\beta, \boldsymbol{\lambda}_h)$ and $(\boldsymbol{\lambda}_\beta^*, \boldsymbol{\lambda}_h^*)$ in the hyperparameter space, if $f(\mathbf{y}|\boldsymbol{\lambda}_\beta, \boldsymbol{\lambda}_h) = f(\mathbf{y}|\boldsymbol{\lambda}_\beta^*, \boldsymbol{\lambda}_h^*), \forall \mathbf{y} \in \mathcal{Y}$, then $(\boldsymbol{\lambda}_\beta, \boldsymbol{\lambda}_h) = (\boldsymbol{\lambda}_\beta^*, \boldsymbol{\lambda}_h^*)$.

The first statement follows from the fact that, conditional on $(\boldsymbol{\beta}, \mathbf{h})$, the likelihood is Multivariate Gaussian with mean $\boldsymbol{\beta}$ and with diagonal covariance matrix $\exp\{\mathbf{h}\}$. Two parameters affect the density in functionally independent ways, thus the statement follows.

To prove the identifiability of the hyperparameter pair $(\boldsymbol{\lambda}_\beta, \boldsymbol{\lambda}_h)$, we proceed by contradiction. Suppose there exist two distinct parameter vectors $(\boldsymbol{\lambda}_\beta, \boldsymbol{\lambda}_h) \neq (\boldsymbol{\lambda}_\beta^*, \boldsymbol{\lambda}_h^*)$ such that $f(\mathbf{y}|\boldsymbol{\lambda}_\beta, \boldsymbol{\lambda}_h) = f(\mathbf{y}|\boldsymbol{\lambda}_\beta^*, \boldsymbol{\lambda}_h^*)$.

By model specification $\boldsymbol{\beta}|\boldsymbol{\lambda}_\beta \sim N(\mathbf{0}, \mathbf{S}\Lambda_\beta \mathbf{S}^T)$ and $\mathbf{h}|\boldsymbol{\lambda}_h \sim N(\mathbf{0}, \mathbf{S}\Lambda_h \mathbf{S}^T)$ where $\Lambda_\beta = \text{diag}(\boldsymbol{\lambda}_\beta^2)$, $\Lambda_h = \text{diag}(\boldsymbol{\lambda}_h^2)$ and \mathbf{S} is the un-differencing operator matrix corresponding to the differencing order k in $\Delta^k \boldsymbol{\beta}$ and $\Delta^k h$.

Using the law of total variance, the variance of y conditional on the hyperparameters

can be decomposed as:

$$\begin{aligned}
\text{Var}(y \mid \boldsymbol{\lambda}_\beta, \boldsymbol{\lambda}_h) &= E_{\boldsymbol{\beta}, \mathbf{h} \mid \boldsymbol{\lambda}_\beta, \boldsymbol{\lambda}_h} [\text{Var}(y \mid \boldsymbol{\beta}, \mathbf{h})] + \text{Var}_{\boldsymbol{\beta}, \mathbf{h} \mid \boldsymbol{\lambda}_\beta, \boldsymbol{\lambda}_h} [E(y \mid \boldsymbol{\beta}, \mathbf{h})] \\
&= E_{\mathbf{h} \mid \boldsymbol{\lambda}_h} [\exp\{\mathbf{h}\}] + \text{Var}_{\boldsymbol{\beta} \mid \boldsymbol{\lambda}_\beta} [\boldsymbol{\beta}] \\
&= \exp\left\{ \frac{1}{2} \text{diag}(\mathbf{S} \boldsymbol{\Lambda}_h \mathbf{S}^T) \right\} + \mathbf{S} \boldsymbol{\Lambda}_\beta^2 \mathbf{S}^T.
\end{aligned}$$

The first term is diagonal, while the second term is dense due to the cumulative sum operation of \mathbf{S} .

The assumption of equal marginal distributions implies equality of variances:

$$\begin{aligned}
\exp\left\{ \frac{1}{2} \text{diag}(\mathbf{S} \boldsymbol{\Lambda}_h \mathbf{S}^T) \right\} + \mathbf{S} \boldsymbol{\Lambda}_\beta \mathbf{S}^T &= \exp\left\{ \frac{1}{2} \text{diag}(\mathbf{S} \boldsymbol{\Lambda}_h^* \mathbf{S}^T) \right\} + \mathbf{S} \boldsymbol{\Lambda}_\beta^* \mathbf{S}^T, \\
\exp\left\{ \frac{1}{2} \text{diag}(\mathbf{S} \boldsymbol{\Lambda}_h \mathbf{S}^T) \right\} - \exp\left\{ \frac{1}{2} \text{diag}(\mathbf{S} \boldsymbol{\Lambda}_h^* \mathbf{S}^T) \right\} &= \mathbf{S} \boldsymbol{\Lambda}_\beta^* \mathbf{S}^T - \mathbf{S} \boldsymbol{\Lambda}_\beta \mathbf{S}^T.
\end{aligned}$$

The left hand side is always diagonal while the right hand side is dense unless $\boldsymbol{\lambda}_\beta = \boldsymbol{\lambda}_\beta^*$.

Hence, the only solution consistent with both sides is when both are zero matrix, implying

$\boldsymbol{\lambda}_\beta = \boldsymbol{\lambda}_\beta^*$ and $\boldsymbol{\lambda}_h = \boldsymbol{\lambda}_h^*$. This is a contradiction to the assumption of distinct parameters:

$(\boldsymbol{\lambda}_\beta, \boldsymbol{\lambda}_h) \neq (\boldsymbol{\lambda}_\beta^*, \boldsymbol{\lambda}_h^*)$. Therefore, the parameters $(\boldsymbol{\lambda}_\beta, \boldsymbol{\lambda}_h)$ are identifiable.

B Full Conditional for Gibbs Sampling

B.1 j

$\mathbf{j} = (j_1, \dots, j_T)$ was introduced to expand the likelihood on $\mathbf{y}^* := (\log(y_1^2), \dots, \log(y_T^2))$.

In this section, we show that $\forall k \in \{1, \dots, 10\}$:

$$\begin{aligned} p(j_t = k | h_t, v_t, s_t, \xi_t, \mu, \xi_\mu, \phi, y_t^*) &= p(j_t = k | h_t, y_t^*) \\ &= \frac{\mathcal{N}(y_t^* | h_t + m_k, w_k^2) p_k}{\sum_{i=1}^{10} p_i \mathcal{N}(y_t^* | h_t + m_i, w_i^2)}, \quad \forall t \in \{1, \dots, T\} \end{aligned}$$

\mathbf{j} is only associated with y^* , which is only associated with \mathbf{h} and \mathbf{j} :

$$p(j_t = k | h_t, v_t, s_t, \xi_t, \mu, \xi_\mu, \phi, y_t^*) = p(j_t = k | h_t, y_t^*) = \frac{f(y_t^* | h_t, j_t) p(j_t = k)}{\int f(y_t^* | h, j_t) f(j_t) dj_t}$$

By Omori et al. [2007],

$$f(y_t^* | j_t, h_t) = \mathcal{N}(y_t^* | h_t + m_{j_t}, w_{j_t}^2)$$

Naturally, $\forall k \in \{1, \dots, 10\}$

$$\begin{aligned} p(j_t = k | h_t, y_t^*) &= \frac{f(y_t^* | h_t, j_t = k) p(j_t = k)}{f(y_t^* | h_t)} \\ &= \frac{f(y_t^* | h_t, j_t = k) p(j_t = k)}{\sum_{i=1}^{10} p(j_t = i) f(y_t^* | h_t, j_t = i)} \\ &= \frac{\mathcal{N}(y_t^* | h_t + \mu_k, \sigma_k^2) p_k}{\sum_{i=1}^{10} p_i \mathcal{N}(y_t^* | h_t + \mu_i, \sigma_i^2)}, \quad \forall t \in \{1, \dots, T\}, \end{aligned}$$

which is what we wanted to show. Exact distribution on $j_t \stackrel{i.i.d.}{\sim} \text{Categorical}(\pi^{\text{Omori}})$ as well as corresponding mean and the variance parameter of each component is described in Omori et al. [2007].

B.2 h

The likelihood and the conditional priors on \mathbf{h} are:

$$f(y^*|\mathbf{j}, \mathbf{h}) = \prod_{t=1}^T \mathcal{N}(y_t^*|h_t + m_{j_t}, w_{j_t}^2) = \mathcal{N}(y^*|h + m_j, w_j^2 I)$$

$$f(\mathbf{h}|\mathbf{v}) = \mathcal{N}(h_1|0, e^{v_1}) \prod_{t=1}^T \mathcal{N}(h_t|h_{t-1}, e^{v_t})$$

Note that \mathbf{h} , a conditionally Gaussian, is a linear combination of $\Delta\mathbf{h}$, with the cumulative sum operator, the precision of the conditional prior of h is a tridiagonal matrix Q_v

$$Q_v := \begin{bmatrix} \left(\frac{1}{e^{v_2}} + \frac{1}{e^{v_1}}\right) & -\frac{1}{e^{v_2}} & 0 & \dots & \dots & 0 \\ -\frac{1}{e^{v_2}} & \left(\frac{1}{e^{v_3}} + \frac{1}{e^{v_2}}\right) & -\frac{1}{e^{v_3}} & \ddots & \ddots & \vdots \\ 0 & -\frac{1}{e^{v_3}} & \left(\frac{1}{e^{v_4}} + \frac{1}{e^{v_3}}\right) & -\frac{1}{e^{v_4}} & \ddots & \ddots \\ \vdots & \ddots & \ddots & \ddots & \ddots & 0 \\ \vdots & \ddots & \ddots & -\frac{1}{e^{v_{T-1}}} & \left(\frac{1}{e^{v_{T-1}}} + \frac{1}{e^{v_T}}\right) & -\frac{1}{e^{v_T}} \\ 0 & \dots & \dots & 0 & -\frac{1}{e^{v_T}} & \frac{1}{e^{v_T}} \end{bmatrix}$$

Since both the likelihood and the prior are Gaussian, the conditional posterior is also Gaussian:

$$f(\mathbf{h}|\mathbf{j}, \mathbf{v}, \mathbf{y}^*) = \mathcal{N}\left(\mathbf{h} \left| \left(Q_v + I \frac{1}{w_j^2}\right)^{-1} \frac{\mathbf{y} - m_j}{w_j^2}, \left(Q_v + I \frac{1}{w_j^2}\right)^{-1}\right.\right).$$

B.3 v

We use the all-without-loop (AWOL) sampler by Kastner and Frühwirth-Schnatter [2014] with parameter expansion on the error term with scale mixture normal distribution for sampling \mathbf{v}, μ and ϕ . By the conditional independence, the likelihood with respect to \mathbf{v} , reduces to $f(\boldsymbol{\omega}^*|v)$ where $\omega_1^* = \log(h_1^2)$ and $\omega_t^* = \log((h_t - h_{t-1})^2), \forall t \geq 2$. With the parameter expansion on the likelihood with 10-component Gaussian Mixture proposed by Omori et al. [2007],

$$f(\boldsymbol{\omega}^*|\mathbf{v}, \mathbf{s}) = \mathcal{N}(\omega^*|v + m_s, w_s^2 I).$$

The conditional prior distribution of v is also Gaussian due to the Z-distribution being a scale mixture Gaussian. \mathbf{v} is also a linear combination of $\mathbf{v}^* = (v_1^*, \dots, v_T^*)'$, where $v_1^* = v_1$ and $v_{t+1}^* = v_{t+1} - \phi v_t, t \geq 2$, conditionally independent Gaussian random variables:

$$\begin{aligned} f(v_1^*|\xi_1, \mu) &= f(v_1|\xi_0, \mu) = \mathcal{N}(v_1^*|\mu, \frac{1}{\xi_1}) \\ f(v_t^*|\xi_{t-1}, \mu, \phi) &= f(v_t - \phi v_{t-1}|\xi_{t-1}, \mu, \phi) = \mathcal{N}(v_t^*|\mu(1 - \phi), \frac{1}{\xi_{t-1}}) \quad t \geq 2, \end{aligned}$$

Similar to section B.2, we have:

$$f(\mathbf{v}|\boldsymbol{\xi}, \mu, \phi) = \mathcal{N}(\mathbf{v}|0, Q_{\xi, \phi}^{-1}),$$

with

$$Q_{\xi, \phi} = \begin{bmatrix} \xi_1 + \phi^2 \xi_2 & -\phi \xi_2 & 0 & \dots & \dots & 0 \\ -\phi \xi_2 & \xi_2 + \phi^2 \xi_3 & -\phi \xi_3 & \ddots & \ddots & \vdots \\ 0 & -\phi \xi_3 & \xi_3 + \phi^2 \xi_4 & -\phi \xi_4 & \ddots & \\ \vdots & \ddots & \ddots & \ddots & \ddots & 0 \\ \vdots & \ddots & \ddots & -\phi \xi_{T-1} & \xi_{T-1} + \phi^2 \xi_T & -\phi \xi_T \\ 0 & \dots & \dots & 0 & -\phi \xi_T & \xi_T \end{bmatrix}$$

Thus,

$$f(\mathbf{v}|y^*, \dots) = \mathcal{N}\left(\mathbf{v} \left| \left(Q_{\xi, \phi} + I \frac{1}{w_s^2}\right)^{-1} \left(\frac{\boldsymbol{\omega}^* - m_s}{w_s^2} + Q_{\xi, \phi} \mathbf{1} \mu\right), \left(Q_{\xi, \phi} + I \frac{1}{w_s^2}\right)^{-1}\right)\right)$$

B.4 s

In section B.2, $\mathbf{s} = (s_1, \dots, s_T)'$ was introduced to expand $\boldsymbol{\omega}^*|\mathbf{v}$. Based on the same argument used in section B.1, $\forall k \in \{1, \dots, 10\}$

$$p(s_t = k | \omega_t^*, v_t) = \frac{\mathcal{N}(\omega_t^* | v_t + m_k, w_k^2) p_k}{\sum_{i=1}^{10} p_i \mathcal{N}(\omega_t^* | v_t + m_i, w_i^2)}, \quad \forall t \in \{1, \dots, T\}.$$

B.5 ξ

Based on Polson et al. [2013], we have

$$v_1 = \mu + \eta_0$$

$$v_t = \mu + \phi(v_{t-1} - \mu) + \eta_{t-1}, \quad \forall t \geq 2.$$

Naturally, $\eta_1 = v_1 - \mu$ and $\eta_t = v_{t+1} - \phi v_t - \mu(1 - \phi)$, $\forall t \geq 2$.

$$f(\xi_0 | \mathbf{v}, \mu, \phi) = \mathcal{PG}(\xi_0 | 1, v_1 - \mu)$$

$$f(\xi_{t-1} | \mathbf{v}, \mu, \phi) = \mathcal{PG}(\xi_{t-1} | 1, v_t - \phi v_{t-1} - \mu(1 - \phi)) \quad \forall t \geq 2,$$

where \mathcal{PG} represents the density function for Polya-Gamma random variable.

B.6 μ

Define $\hat{v}_\phi^* = \frac{\sum_{t=2}^T \sqrt{\xi_t} (v_t - \phi v_{t-1})}{(1-\phi) \sum_{t=2}^T \sqrt{\xi_t}}$, so that

$$v_t - \phi v_{t-1} | \boldsymbol{\xi}, \mu, \phi \sim N((1-\phi)\mu, \frac{1}{\xi_t})$$

$$\hat{v}_\phi^* | \boldsymbol{\xi}, \mu, \phi \sim N(\mu, \sigma_{\xi, \phi}^2)$$

$$\sigma_{\xi, \phi}^2 = \frac{T-1}{((1-\phi) \sum_{t=2}^T \sqrt{\xi_t})^2}.$$

The conditional prior distribution on μ also reduces to $f(\mu | \xi_\mu) = \mathcal{N}(\mu | 0, \frac{1}{\xi_\mu})$. Thus, the conditional posterior distribution for μ is

$$f(\mu | \hat{v}_\phi^*, \boldsymbol{\xi}, \xi_\mu, \phi) = \mathcal{N}\left(\mu \left| \left(\frac{1}{\sigma_{\xi, \phi}^2} + \xi_\mu\right)^{-1} \frac{\hat{v}_\phi^*}{\sigma_{\xi, \phi}^2}, \left(\frac{1}{\sigma_{\xi, \phi}^2} + \xi_\mu\right)^{-1}\right)\right).$$

B.7 ξ_μ

Based on the scale mixture representation of the Z-distribution Polson et al. [2013]:

$$f(\xi_\mu | \mu) = \mathcal{PG}(\xi_\mu | 1, \mu).$$

B.8 ϕ

Unlike other parameters, ϕ is not conditionally conjugate to its likelihood. Thus, the slice sampling method Neal [2003] is used for the MCMC sampling. By taking the linear transformation of v_t , Let's consider its likelihood becomes $\hat{v}_\mu := \frac{1}{T-1} \sum_{t=2}^T v_{\mu,t}$, where $v_{\mu,t} = \frac{1}{2} \left(\frac{v_t - \mu}{v_{t-1} - \mu} + 1 \right)$. We have the following conditional likelihood and prior for ϕ :

$$f(\hat{v}_\mu | \mu, \boldsymbol{\xi}) = \mathcal{N} \left(\hat{v}_\mu \left| \frac{\phi + 1}{2}, \frac{1}{(T-1)^2} \sum_{t=2}^T \frac{1}{4\xi_{t-1} (v_{t-1} - \mu)^2} \right. \right)$$

$$f\left(\frac{\phi + 1}{2}\right) \sim Beta\left(\frac{\phi + 1}{2} \left| 10, 2 \right. \right)$$